Università degli Studi di Napoli *Federico II*

DOTTORATO DI RICERCA IN FISICA

Ciclo XXXIV

Coordinatore: prof. Salvatore Capozziello

Study, realization and characterization of new solid state devices for particulate matter and pollutant gases for the Air quality monitoring.

Settore Scientifico Disciplinare FIS/07

Dottorando
Luigi Barretta

Tutor
Prof. P. Maddalena
Dott. E. Massera
Dott. T. Polichetti

Anni 2018/2022

ABSTRACT

The need to know, and therefore measure, the quality of the air we breathe and live in is vital, as this could affect our health conditions and certainly affects our lifestyles. Pollutant gases, resulting from natural or human processes, are potentially harmful to human health and to the surrounding ecosystem where these are released. In addition to gases dissolved in air, a source of pollution whose interpretation is still vague but certainly has a strong impact on health is that related to atmospheric particulate matter. Recent urban systems, very dynamic and frequently changing, would require a high spatial density of measurements and with sampling time congruent with the dynamics to be studied (seconds, minutes, hours). Currently, accredited instruments for air quality measurements require long sampling times, highly trained personnel, and, given their bulk and cost, are spatially distributed with low density.

Major electronic device manufacturers, and in particular environmental sensor manufacturers are pushing toward miniaturization of devices so that they are portable and cost-effective, compatible with IOT scenarios.

On the other hand, it is necessary to know the degree of reliability of the information generated by these devices for air quality measurement. Unfortunately, miniaturization and increasingly rapid sampling are at the expense of the precision and accuracy of measurements. The lack of regulations related to this type of devices today does not allow them to be used as an aid to official instruments to improve the definition of spatio-temporal pollution maps. The scientific literature, however, demonstrates the potential of such

devices to be of assistance in understanding better the state of air pollution in our urban centers. In the future, these devices, in concert with official strumantazioni, will have the task of integrating report and implement other devices to contribute to the improvement of the air quality of both indoor and outdoor environments.

The objective of this thesis, concerns the design the study and optimization of portable devices based on solid-state sensors capable of measuring the concertation of gases and atmospheric particulate matter in the air.

The main results, which will be shown in the appropriate sections, are: The realization and use of a characterization chamber for atmospheric particulate sensors, installed in the ENEA Laboratories (partners in this thesis);

The study in a controlled atmosphere of commercial devices for low-priced atmospheric particulate matter (commonly known as Low-Cost PM Sensors) and the publication in collaboration with ENEA of a review on Low-Cost PM Sensors;

The characterization of innovative devices based on piezoelectric materials provided by STMicroelectronics (partner as well as funder of this thesis project) in the presence of atmospheric particulate matter.

CONTENTS

INTRODUCTION

The growing diffusion of technological devices supporting human activities and the consequent rise in the demand for electricity production has led to the increase of the pollution in the large industrial areas. An additional source of atmospheric pollution, mostly concentrated in large urban areas, is related to transport. Two types of pollutants have a major impact on air quality:

- The first one is represented by the atmospheric particulate matter (PM), formed by particles of variable size which can have serious consequences on human health if inhaled. The attention on this kind of pollutant suddenly increased during the COVID-19 pandemic because there is a well-founded suspicion of a possible correlation between PM and the spread of the SARS-COV2 virus.

- The second class of pollutant is represented by harmful gases, which constitute a serious risk, sometimes even fatal, for those who inhale them.

The growing concern about the health consequences of exposure to air pollutants has pushed more and more communities, all over the world, to get informed and to take precautions by intervening both on regulations and on the citizens' behavior, a change in attitude driven and accelerated exponentially by the spread of the Internet.
On the basis of the studies produced and the social drive, the organizations in charge of monitoring air quality have the arduous task of readjusting the

regulations and methods of controlling the concentration limits. Currently, the concentration of harmful pollutants is controlled in a very similar way around the world through monitoring stations using specific standards. These stations, however, are very limited in number on the territory; consequently, the information collected refers to macroscopic areas (we are talking about square kilometers). For this reason, these tools are to be considered obsolete, given that, today, very different scenarios are configured in the city at much shorter distances than those monitored by the control units. Another problem is that these stations provide information on very long temporal averages (hours, days), so they are not able to reflect very dynamic contexts such as that of a large city.

Having said that, it is clear that the information gathered from the aforementioned monitoring stations is lacking and this pushes the scientific community and companies that develop electronics and sensors to invest in innovative solutions.

Even more complicated is the issue of indoor air quality where there are no regulations in terms of monitoring stations, a serious problem considering that most of the time is spent indoors.

A breakthrough could be the introduction of portable solid state devices, which would help thicken the network of sensors that measure the concentrations of the pollutants, as well as reduce sampling times thus providing timely information.

This thesis addresses all the above issues and is part of the S.A.L.VO. project, which involves the construction of a portable device capable of monitoring concentrations of atmospheric particulate and harmful gases for the safety of workers.

In the next section, in addition to illustrating the objectives of the project, we will discuss the regulations concerning air quality; subsequently we will focus on the measurement methods and on the characterizations carried out on commercial and prototype devices that fall within the scope of the project. In the first chapter, dedicated to the particulate matters, we will describe the measurement methods also presenting the state of the art of the devices currently available on the market. In the section 1.5.2 we will discuss the

differences between laboratory tests and tests on the field of the PM sensors; we will then move on to illustrate one of the main objectives of this work, namely the design and the construction of a PM characterization chamber built in the ENEA research center in Portici.
The second chapter will be devoted to piezoelectric materials, and then after a brief introduction to these materials and its applications in the field of sensors will be described the tests to assess whether such a device can be used as a sensor of PM.

S.A.L.VO. Project

The World Health Organization and Europe Mortality databases in 2011 in Europe have estimated that 7200 cases of respiratory diseases are related to occupational exposure to VOCs and particulate matter. The latest Annual Reports of the National Institute for Insurance against Accidents at Work (INAIL) confirm the European trend, putting respiratory diseases in Italy in third place (13.5%) among occupational diseases and also underlining the seriousness of their consequences. Volatile organic compounds (VOCs) and dusts constitute within work environments one of the highest causes of asthma, lung cancer, chronic obstructive pulmonary disease (OPD) and respiratory tract infections.
As of 2014, there has been an alarming increase in respiratory illnesses in sectors such as agriculture, transportation, and mining. These data confirm the importance of wearing appropriate Personal Protective Equipment (PPE) that prevents operators from inhaling hazardous substances and particulates. There is therefore an increasingly urgent need to increase the well-being of workers, making them feel greater satisfaction, security and inclusion in the factory and in the workplace in general. In the analysis of the issues related to safety in the workplace, the scientific literature has highlighted what is already expected: the added value coming from an "Internet of Things" (IoT) approach can mean a decisive paradigm shift in the methodologies of the safety management in the workplace, resulting in the net decrease in the rate of accidents. The central point is that the current technology enabling

this scenario has limited or even lacking possibilities in the part relating to the devices that must allow the worker to interact with the surrounding environment.
The project within which this thesis work is developed, called S.A.L.VO. (Realizzazione di un nodo multiSensore per il monitoraggio degli Ambienti di LaVOro), a PON project involving ENEA and STMicroelectronics as partners, expiring in December 2023; purpose of the project is the realization of a multisensory node for the realization of individual protection devices for workers, responds to this criticality, aiming to create a multi-sensor node for continuous monitoring of the worker in relation to the environment in which he operates, with reference to both his physical parameters (location, activity) and those of the surrounding environment (harmful gases and noise). As part of this project, it was envisaged that the information provided by the sensors should then be sent to an Internet of Things (IoT) service platform that integrates and synthesizes the information coming from the various nodes, enriching its semantic value through Artificial Intelligence (AI) approaches. In this vision, the information and data acquired must be made available both to the user and to the upper management levels, through the development of a Smart PPE that will allow, in near real time, the reconstruction of the working environment as a whole; this portable multisensor node was designed to consist of environmental, gas and particulate sensors, physical, inertial and audio sensors, capable of immediately communicating potential alarm situations to the user even on a mobile phone.
Environmental sensors are designed to assess a person's exposure to stresses such as RH / T and gases such as VOC, CO_2, O_2 and CO in concentrations in the air that are dangerous for the person, or possibly to particulate matter. In addition, inertial sensors serve to identify "man down" situations or other types of movements that may be a source of danger to workers. Finally, audiometric sensors have to assess daily noise exposure and track any exposures that exceed the allowable noise level. In a "short range" scenario, the data collected by the Smart PPE, will be sent to a smartphone-like system, BLE 2.0 or, preferably, with Bluetooth Low Energy (BLE) and WiFi, and then sent to a server on which support and decision-making functions can be

implemented. In the case in which we move in the outdoor "long range" the smart DPI will be able to send data directly and autonomously to the server through the Lora/SigFox protocol. Most of the sensors are already commercially available, but some of them, in particular those for gas and particulate, have been developed within the project. Those sensors have been designed in order to minimize their consumption and make their manufacturing processes compatible with the other (physical) sensors that will make up the final node with the aim of being able to conceive, at the end of the project, a chip that integrates both physical and chemical sensors, achievable with ST's proprietary technologies (CMOS compatible). The technological solutions of the project were defined through two objectives, part of which pursued during the experimental thesis activity:

1. Design and implementation of Particulate and Gas sensor modules
   Some of the functionality of the Smart DPI device is based on solutions currently in the STMicroelectronics portfolio. This technological objective will be developed

   - A new gas sensor based on NDIR (Non-Dispersive Infra-Red) technology
   - A new particulate matter sensor

   NDIR Gas Sensor
   An NDIR gas sensor specifically measures the gas concentration in a sample chamber. If there are gases in the path from an infrared light source to a detector, then, in a non-dispersive system, light is absorbed by the gases. How much light is absorbed is a function of how much gas is between the light source and the light detector. The infrared light source is installed at one end of an enclosure and the light detector is installed at the opposite end. The light detector has a filter so that it specifically detects light in the electromagnetic spectrum related to CO_2. The input and output between the light source and the detector allow CO_2 to move freely in and out of the enclosure. It is clear from the mechanism of operation, that the sensor can 'extend

its functionality to all gases that have absorption in the infrared ray from 3 to 10μm, many of which are harmful and present in the working environment such as carbon monoxide (CO), ammonia, methane, etc. The feasibility study and implementation reported in this project can be potentially extended to a wider plethora of gases harmful to human health.

Particulate sensor

Another element that is strongly harmful to human health is particulate matter, with particular reference to particles with a diameter of less than 10μm, defined as inhalable particles. These small particles can be inhaled causing serious damage to human health. The table shows the permitted levels of particulate matter $PM_{2.5}$and PM_{10}above which there are harmful effects on health. Given their highly damaging characteristics, the development of particulate sensors has been of considerable importance in recent years. The atmospheric particulate sensor to be developed in this project is based on the idea of separation of atmospheric particulate matter by centrifugal force and subsequent detection by capacitive sensors. The advantages of such a system are many and put the device designed significantly ahead of the technological and industrial state of the art. In fact, the most common types of atmospheric particulate measuring devices are mainly based on "impact" mechanisms for particle size separation and on optical approaches for measuring the number of particles in the collected air volume. These strategies, although resulting in high-performance devices, are, however, poorly integrable because of the necessary optical structures and require structural and functional complications related to the need to clean the surfaces affected by atmospheric particulate matter. These problems remain also in the case of less conventional solutions based for example on electrophoretic techniques for particle size separation. The solid-state particulate sensor will consist of four main blocks: air sampling, flow management, particle separation, and particle detection.

2. Realization of an IoT Node for Smart PPE The sensors that will constitute the final portable device (the commercial ones and that developed ad hoc for gas and particulate) will be integrated on an IoT Node that with appropriate communication protocols will send data to an IoT cloud implemented to provide monitoring services of the working environment and decision support to users through mobile or web applications. The system architecture is schematized in the Figure below: The system architecture consists of an array of sensors connected to the "safety lab" which incorporates the front-end electronics for processor input, power source, data storage capability, user interface, and communication channels required for the application. At the core of the safety, the lab is a low-power microcontroller (ARM Cortex M4) used for power management, user interaction, real-time signal processing (embedded algorithms), data fusion (edge computing), short-range BLE/WiFi and long-range LORA/SF communication, etc. In the first phase, we will use boards of the STM32 Nucleo family equipped with Lora/SIgFox or BLTE communication modules equipped with related STEVAL (evaluation board kit) of existing sensors (IMU, RH, T, Audio, VOC), commercial particulate and NDIR sensors or the modules developed at an early stage in 1).

This Project will culminate in the delivery of a prototype that will be tested in a laboratory scenario. This will be followed by the development and testing of the multisensor node and its SW platform, with the integrated system for the microcontroller, sensors, communication modules, design optimization, characterization and development of readout circuits for the sensors that will conclude the workflow. Bluetooth connectivity will require the development of specific firmware for the ST sensors and the communication module via SPI with the ST microcontroller. ST electronic components will be mainly used with solutions for RF communications, power management, and STM32 microcontrollers to provide the board with the capability of onboard processing. In this second phase, we will also use the particulate and NDIR sensor modules developed in step 1.

ACKNOWLEDGMENT

Research reported in this publication was supported by S.A.L.VO. project that has received funding from the National Programs (PON) of the Italian Ministry of Economical Development (MISE): code B48I20000050005 (Prog n. F/190012/01/X44).

CHAPTER

ONE

PM SENSOR

The following chapter discusses particulate matter sensors. Its content is a summary of the review [1] (of which I am a co-author) to which we refer for more completeness.
In the chapter after a definition of what is commonly known as PM, we will give space to the regulations on the measurement of this pollutant and then to what are the official and unofficial methods of measurement. Will then be introduced to the low-cost commercial sensors for which will be given an in-depth look at their principle of operation and what is the current state of the art.
Finally, the realization of the test chamber for particulate sensors installed in the ENEA research center in Portici and the related tests on commercial sensors carried out during this work will be discussed.

1.1 PM definition

The air we breathe always contains a certain amount of solid matter that comes from natural sources such as soil, windblown dust, pollen, etc. or from human activities related to its misuse such as combustion fumes and construction work, etc.
The past century has been one of unprecedented technological progress and

industrialization. The products of this phenomenon such as industries, the automotive sector and transport in general, and intensive animal breeding to ensure the needs of communities have increased and modified the composition of this solid matter suspended in the air, especially in large cities where the phenomenon is increasingly evident. The impact that this phenomenon can have on human health has prompted many countries to regulate phenomena related to the sources of atmospheric particulate matter (e.g., traffic blocks) and to provide air quality standards (this is not only related to atmospheric particulate matter but also to noxious gases).

The Clean Air Act of 1970 was one of the first acts in terms of regulating the phenomena related to the quality of breathing air, regulating the standards set for six different types of pollutants. Since then, air pollution has been regulated worldwide through a series of laws and regulations [2].

Atmospheric particulate matter is one such pollutant and is defined as the set of solid, liquid, or a combination of solid and liquid particles in the environment. This is classified according to the particle diameter [3]. In this act, the regulations were based on the mass of suspended particles of any size, i.e., total suspended material (TPS). These regulations took into account the mortality associated with short-term pollution episodes. The first standard included both an annual average standard of $75\mu g/m^3$and a maximum daily average standard of $260\mu g/m^3$not to be exceeded at any time during the year. However, these criteria are being revised in tandem with studies conducted on the influence this pollutant has on health, specifically, how particle diameter affects lung disease and the like in different ways.

In 1980, the Council of the European Communities gave Directive 80/779/EEC. However, the first clear and comprehensive definition of $PM_{10}$was given in the late 1980s by the U.S. Environmental Protection Agency (EPA), which is developing the National Ambient Air Quality Standard for the fraction of suspended particulate matter with an aerodynamic size less than $10\mu m$ [4] established its limit values. This standard was updated later (10 years later) also for $PM_{2.5}$after a long research on how the "fine" atmospheric particulate matter affected human health. The European community, following these directives, implemented similar measures in 1996 with Directive 96/62/EC for

Table 1.1: Current exposure standards to $PM_{10}$and $PM_{2.5}$

	$PM_{2.5}(\mu g/m^3)$		$PM_{10}(\mu g/m^3)$	
Averaging time	**24h**	**annual**	**24h**	**annual**
EU (1)	-	25	50	40
USA (2)	35	12	150	-
China (3)	75	35	150	70
Hong Kong (4)	75	35	100	50
Japan (5)	35	15	100	-
Australia (6)	25	8	50	25
WHO (7)	25	10	50	20

(1) 2008/50/EC Directive on Ambient Air Quality and Cleaner Air for Europe.
(2) EPA Timeline of Particulate Matter
(3)Ambient Air Quality Standards (GB 3095–2012) and Technical Regulation on Ambient Air Quality Index (HJ 633–2012, on trial) from the website of the Ministry of Environmental Protection, China.
(4) "Air Quality Objectives". Environmental Protection Department, Hong Kong. 19 December 2012.
(5) Environmental Quality Standards in Japan - Air Quality.
(6) Department of the Environment (25 February 2016). "National Environment Protection (Ambient Air Quality) Measure". Federal Register of Legislation.
(7) Ambient (outdoor) air pollution

PM_{10}, while monitoring of the $PM_{2.5}$fraction started in 1999 with the Directive (1999/30/EC).

Similar to the definition of PM_{10}, $PM_{2.5}$is defined as a particle fraction captured with 50% efficiency at $2.5\mu m$. Directive 99/30/EC establishes the methodology for the assessment of PM_{10}concentrations, either through a reference method for sampling and measurement (CEN standard EN12341(3)) or through the use of instruments demonstrated to be equivalent to a reference instrument.

Current limits for allowable concentrations of $PM_{10}$and $PM_{2.5}$in major industrialized countries/geographic areas are shown in the table 1.1 along with WHO guidelines.

Limit values for $PM_{10}$and $PM_{2.5}$are derived from human epidemiological data; laboratory data from animals and in vitro cultures are used for support

purposes only [5].

1.2 PM sources

The effects on human health are, of course, not only related to the physical properties (such as size and shape) of the particles but are also related to the chemical properties (such as composition, solubility, oxidation capacity, etc.).
The above physical properties give information about the degree to which particles penetrate the respiratory system, it is easy to realize that the smaller the particles, the more penetrating they are. The chemical properties give information about how the atmospheric particulate matter may react with other factors involved, be they other pollutants or the organs to which it attaches.
The chemical composition of particulate matter is extremely heterogeneous it can contain both organic and inorganic compounds, acids, metals, etc. This composition is, of course, dictated by the source of emission of the particulate matter itself, which may be natural or a waste product resulting from human activities. As shown by Snider et al [6]. In Europe, the main sources of PM emissions (both $PM_{10}$and $PM_{2.5}$) are due to combustion processes, such as fuel combustion (transport) and combustion used in commercial, institutional and domestic heating [7].
Especially in the emission of fine particulate matter, there is an incidence of waste products from the combustion of black coal [8]. Particulate matter is, in addition, often coated with compounds of organic and inorganic nature [9], as may be the case with compounds resulting from the use of catalytic converters in automobiles, which use metals that may lead to the presence of platinum (Pt), palladium (Pd), and rhodium (Rh) in their emitted particulate matter [10].
Natural sources of atmospheric particulate matter, such as volcanic eruptions, are also richer in sulfur particles. Of course, each particulate source has its emission profile and characteristic particle size, as well as its chemical composition. The tablreftable2 provides a brief overview of which are the

most common sources of atmospheric particulate matter and what are the characteristic particle sizes emitted by these sources (data in these tables are taken from [11]).

1.3 Measurement techniques

To obtain a correct measurement of the concentration of $PM_{10}$and $PM_{2.5}$, it is necessary to unambiguously define what is meant by the size of the particles forming the particulate matter. Particles, of course, do not have perfect spherical shapes but are affected by irregularities. The particle size of x μm generally refers to the aerodynamic diameter, i.e., the equivalent diameter of a spherical particle with a density of $1 g/cm^3$ having the same settling velocity as the irregular particle.
It should be remembered that particulate matter refers to a measure of concentration and therefore to a mass per unit volume. Since PM is represented by a class of particles with different sizes and distributions, when referring to total mass one must take into account that particle mass increases with the third power of the diameter for the same volumetric mass density. It is easy to realize that larger particles contribute more to the total mass determination figure1.1. UNI EN 12341: 2014 and EPA 40 CFR PART 50 standards govern the reference measurement The method, which relates to materials and how to use them, consists of using a sampling head to select particles based on their size (PM_{10}or $PM_{2.5}$), using a filtering system to collect the particulate matter. Next, we focus on the gravimetric mass determination of the sampled PM. The overall measurement system site consists of two main parts: the sampling system and the analysis and control system.
The first stage is sampling, in which ambient air is drawn in and, relying on fluid-mechanical techniques, such as direct impaction, virtual impaction, cyclonic filtration, etc., separated according to their size. An example of an air sampler is presented in the figure 1.2. Airflow sampling is controlled by control devices that set the flow rate and maintain it at time intervals. The sampling head and its specifications are regulated by international agreements, it can separate the dust according to its size going to select the particulate

Table 1.2: The most common sources of PM with the types of related PM emitted.

Source		**PM Size**	
Biomass burning	Beech burning	PM_{10}	
	Hard woodburning	PM_{10}	
	Larch burning	PM_{10}	
	Leaves burning	PM_{10}	
	Oak burning	PM_{10}	
	Olive oil burning	PM_{10}	$PM_{2.5}$
	Pellet burning	PM_{10}	
	Natural gas burning	PM_{10}	$PM_{2.5}$
	Wood burning	PM_{10}	$PM_{2.5}$
Fossil fuels	Coal burning	PM_{10}	$PM_{2.5}$
	Coke burning	PM_{10}	$PM_{2.5}$
	Boiler	PM_{10}	$PM_{2.5}$
	Refineries	PM_{10}	
Industrial	Ammonium nitrate	PM_{10}	$PM_{2.5}$
	Ammonium sulfate	PM_{10}	$PM_{2.5}$
	Iron and steel prod.	PM_{10}	$PM_{2.5}$
	Metal smelting	PM_{10}	$PM_{2.5}$
	Fertilizer prod.	PM_{10}	$PM_{2.5}$
	Cement	PM_{10}	$PM_{2.5}$
	Ceramic	PM_{10}	$PM_{2.5}$
	Foundries	PM_{10}	$PM_{2.5}$
Natural dust	Marine aerosol	PM_{10}	$PM_{2.5}$
	Volcanic dust	PM_{10}	
	Brake dust	PM_{10}	$PM_{2.5}$

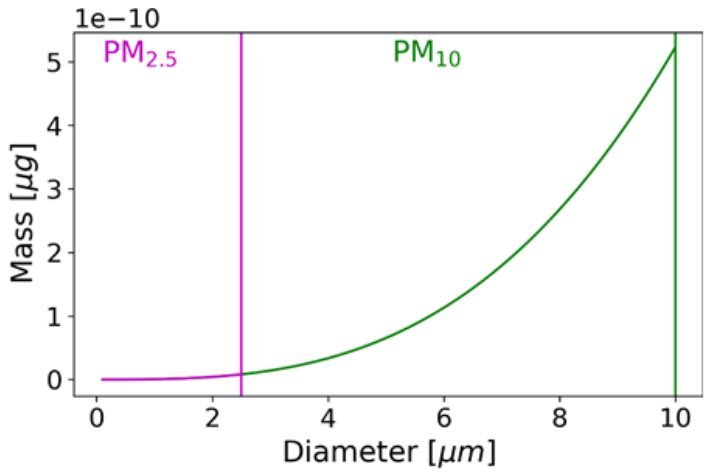

Figure 1.1: Mass particle vs diameter for the two classes of particulate ($PM_{2.5}$in purple and PM_{10}in green)

matter of interest, $PM_{2.5}$and PM_{10}, with an efficiency of 50%.
This sampling operation takes 24 hours with a low volume sampling flow, approximately $1m^3/h$. The filter membranes have adequate porosity and are made of different materials (quartz, fiberglass, Teflon, cellulose esters, etc.) depending on the type of chemical characterization required for the PMsample. After the sampling step, the particulate concentration is estimated in the laboratory. The filters are brought to controlled temperature and humidity, $20 \pm 1°C$ for temperature and $50 \pm 5\%$ for relative humidity, and then weighed using an analytical balance.
The variation in filter mass, given the amount of volume sampled, gives us a measure of particulate concentration that is generally expressed in $\mu g/m^3$. Measurements of fine particulate matter, and in particular those of $PM_{2.5}$, even using this equipment standard suffers from significant variability. This variability, besides being caused by the different sampling systems, is affected by the fact that the chemical composition of these small particles is semi-volatile.
$PM_{2.5}$can be formed, for example, by ammonium nitrate and organic compounds. For this reason, the particle loss in fine particulate measurement can be much greater than in PM_{10}[12]. The main disadvantage of the gravi-

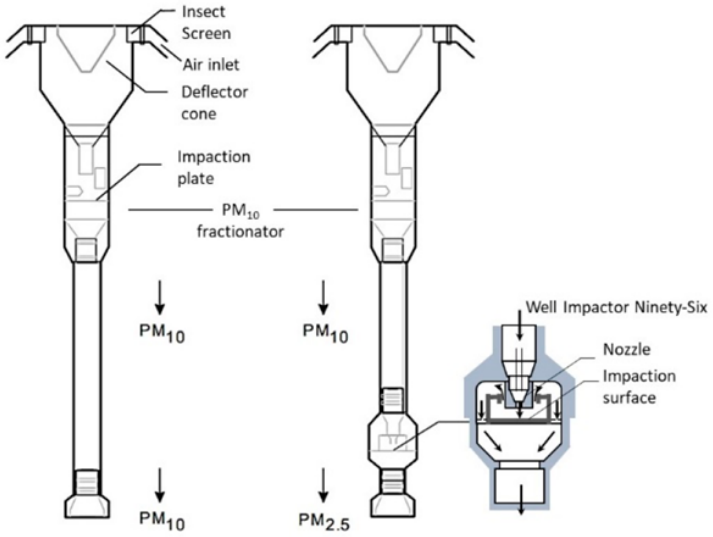

Figure 1.2: Schematic of a standard low-vol PM_{10}inlets aspirating at 16.7 lpm (actual conditions). On the right the schematic of a sampling head equipped with $PM_{2.5}$aerosol fractionation using a good impactor ninety-six (WINS)

metric method is that it returns a particulate measurement every 24 hours, however, anticipated it may be important to instead obtain real-time information in scenarios where there are sudden changes in concentration rates. Automated methodologies have been explored to enable continuous measurements, and numerous techniques have been developed and tested, but few techniques have demonstrated equivalence to the reference method described above. Equivalent methods using gravimetric determinations include tapered oscillating element microbalance (TEOM) and beta ray attenuation (BAM, which is not strictly gravimetric but is assimilated as such). The sampling system used in the equivalent methods uses the same size-selective inputs for PM_{10}or $PM_{2.5}$as for the reference method.

A TEOM makes use of a microbalance system. The conical element consists of a filter cartridge mounted on the tip of a hollow glass tube. The base of the tube cannot move, while the tip is free to vibrate at its natural frequency. As the particulate matter in the air is collected on the filter

cartridge, the natural frequency of oscillation of the tube decreases. The mass detected by the sensor is then the result of measuring the frequency change: the electronic circuit detects this change and calculates the particle mass rate from the magnitude of the frequency change. The element is periodically cycled back to its natural frequency. To account for humidity or volatile PM components in the sampled air, and added dynamic filter measurement system (FDMS) is usually implemented. This system considers the dynamics of the PMdeposited on a cooling filter and how this material behaves over time. The flow alternates between baseline and reference sampling periods via switching valves. Since TEOM monitors are based on the frequency of a sensitive oscillating element, mechanical noise can interfere with the calculations. In addition, large temperature fluctuations can also cause microbalance errors.

A second system that is considered equivalent is the beta attenuation monitor (BAM), which uses the principle of β-ray attenuation to measure the mass concentration of PM in ambient air. Air is drawn in at 16.7 L per minute through a PM_{10}inlet followed by the use of a VSCC (Very Sharp Cut Cyclone) particle separator to remove particles larger than 2.5 µm for $PM_{2.5}$monitoring. The sample stream then passes through a glass fiber filter belt. A carbon-14 (^{14}C) element above the filter belt constantly emits β particles, which are detected and counted by a scintillation detector below the filter belt. At the beginning of each sampling period, the BAM counts the attenuated β-rays from a new, unsampled filter tape spot. The sample is then filtered through that belt spot. At the end of the sampling period, the BAM counts the β-rays attenuated by the filter tape spot loaded with the sampled PM. The difference in the degree of attenuation between the pre- and post-sampled filter tape is directly proportional to the mass of PM in the sampled air. The mass concentration in $\mu g/m^3$is obtained by dividing the mass of $PM$by the total volume of air sampled.

Beta attenuation analysis also uses an equivalent PMmonitor, which combines field-proven sequential sampling technology with BAM measurement principles. The unique feature of this type of instrument is the presence of two separate inlets and two flow lines with filter holders, which are inde-

pendently controlled and operate simultaneously. This configuration allows $PM_{2.5}$and $PM_{10}$to be sampled and PMconcentration results to be obtained on an hourly basis. Another equivalent method of PMmeasurement is the Synchronized Hybrid Ambient Real-Time Particulate Monitor (SHARP), which combines the accuracy of β-ray attenuation monitors with the high temporal resolution of nephelometers. In this hybrid system, the sample stream first passes through the nephelometer where a sensor measures the light scattering caused by the particle aerosol as it passes through an $880nm$ illumination beam. Next, the aerosol is deposited onto a filter belt. Here, the instrument measures particulate concentrations by passing radiation through a known sample to the detector, similar in principle to BAM, reporting β-counts according to a reference standard. Light scattering is another important technique usually used to measure PMdistribution. This technique is used to perform real-time equivalent measurements of $PM$with the precision and accuracy of a FEM instrument. This technique and its basic principles will be outlined in more detail in the next section.
An accurate list of references and equivalent instruments for PM measurements can be found in [13].

1.4 LCPMS: low-cost PM sensor

As anticipated, the measurement methods analyzed to date require the collection of PMover a very long period, of at least 24 hours. In recent decades, there has been an increasing public demand for personal, near real-time air quality monitoring. As a result, an increasing number of low-cost particulate matter sensors suitable for IoT tool development have appeared. According to the definition introduced by US EPA, low-cost PMsensors are characterized by costing less than $1000 and are equipped with miniaturized electronics [14]. Due to their low cost, these sensors are poorly documented and not certified. This lack of information has generated interest in the scientific literature on the ability of these classes of sensors to measure PM. Several scientific articles have evaluated the properties of these sensors. The table 1.3 provides a current list of global LCPMS manufacturers and the number

of different models of PMsensors they provide, along with the number of scientific articles that have studied their performance, both under laboratory and field conditions. Next, the results of this experimental activity will be

Table 1.3: Worldwide LCPMS manufacturers, the number of different PMsensor models they offer, and the number of scientific papers that have investigated their performance, either in laboratory conditions or in the field.

Manufacturer	Number of Sensor Models	References in This work
Alphasense	3	12
Honeywell	3	3
Sharp	2	10
Amphenol Advanced Sensors	6	NA
NanoSense	1	NA
Shinyei	5	3
Bjhike	1	NA
Inovafitness	2	3
Tianjin Figaro-isweek	1	NA
Cubic Sensor and Instrument Co Ltd.	11	NA
Panasonic	2	NA
Winsen	3	2
EcologicSense	1	NA
Plantower	3	9
Yaguchi Electr. Corp.	1	NA
Elitech	1	NA
Samyoung S&C	2	1
Grove Studio	1	NA
Sensirion	1	1

reported to extract a roadmap for a better understanding of the uses and capabilities of these types of devices for rapid air quality assessment, and characterizations of these same devices in the particulate chamber built by ENEA will also be shown, aspects of which will be discussed in more detail later. In particular, all the LCPMSs reported above are optical sensors based on a different operating mechanism than the sensors analyzed in the previous section. Therefore, to understand the limitations and capabilities of this class of devices, we must first clarify how their results can be compared to the standard measurement systems reviewed above. LCPMSs are a miniaturization of optical particle counters (OPCs) that use light scattering to measure PMdistribution, according to Mie's theory [15]. In the following, the physical principles of operation of these sensors are discussed and OPCs are described.

1.4.1 Mie theory

When a particle passes through a beam of light, the light is deflected from its natural path, giving rise to the phenomenon of scattering; this phenomenon can be exploited to detect the passage of particles and provides the basis for the operating mechanisms of OPCs. As is well known, scattering is a conservative process resulting from three cumulative effects: reflection, refraction, and diffraction. Many theories proposed during the nineteenth century attempted to explain light scattering, but they were valid only for particles of certain sizes and shapes and were applicable only in certain media. in the early twentieth century, Gustav Mie developed a general theory that rigorously described light-particle interactions for spherical particles of all sizes dispersed in any medium. The characteristic intensity of scattered light as the angle varies is accurately predicted by this theory; by analyzing this characteristic, the particle size distribution can be determined. The assumptions on which this theory is based are elected below:

- Light is monochromatic and composed of plane waves.
- The particles are spherical and isotropic.
- Both scattering and absorption are taken into account.
- Considering a low concentration of particles it is assumed that light scattered from one particle to another is negligible.
- The diffusion characteristics considered are independent of the motion of the particle.
- Quantum effects are not considered.

In Figure 1.3, we schematize what are the possible light-beam-particle interactions in terms of the relative distance between light beams and particles. In particular, except for absorption, the light beam continues its path unaltered if it is far enough away from the particle; as the distance decreases, the deviation becomes more and more pronounced, going from a deviation of a few degrees to a 180° inversion. The intensity of scattered light is a function

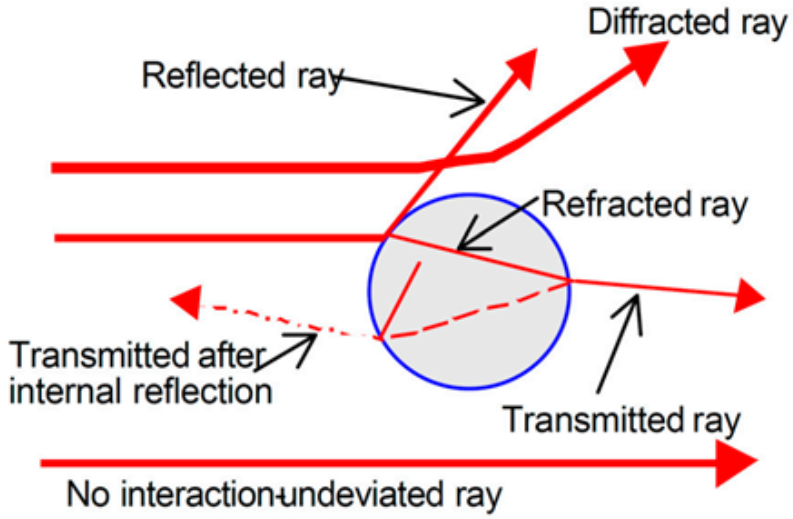

Figure 1.3: The potential interaction between a beam of light and an isolated spherical particle.

of wavelength λ, scattering angle Θ, particle size d, and the relative refractive index n of the particle and medium as shown by the following relationship:

$$I_{sc} = I_{sc}(\Theta, \lambda, d, n) \tag{1.1}$$

Mie theory precisely describes scattering when the angle and refractive index of the material are fixed. Due to the complexity of the relationship between the parameters involved, a simplified form is generally preferred, which depends on the size of the particle concerning the wavelength of the incident light.
By introducing the size parameter α, defined by.

$$\alpha = \frac{\pi d}{\lambda} \tag{1.2}$$

We separate three distinct diffusion regimes due to this parameter:

$\alpha \sim 1$ one is in the Mie solution regime, and a detailed approach is required [16]. The most notable features of these results are Mie resonances with dimensions that diffuse particularly strongly or weakly.

$\alpha \ll 1$ we are in the presence of Rayleigh scattering, which describes the scattering of particles much smaller than the wavelength of the incident light. In this approximation:

$$I_{sc} = I_{inc} \frac{1 + \cos^2 \Theta}{2R} \left(\frac{2\pi}{\lambda} \right)^4 \left(\frac{n^2 - 1}{n^2 + 1} \right)^2 \left(\frac{d}{2} \right)^6 \tag{1.3}$$

where I_{sc} is the intensity of the scattered light, I_{inc} is the intensity of the incident light, Θ is the scattering angle, and R is the distance between the particle and the light beam. The above expression returns a dependence on the sixth power of the diameter in this regime.

$\alpha \gg 1$ we are in the presence of simplified geometric scattering:

$$I_{sc} = I_{inc} K(n, \Theta) d^2 \tag{1.4}$$

That said, and to ensure that the intensity of the scattered light is proportional to the diameter of the particles to be detected (0.1-100μm), optical particle counters are equipped with light generators in the visible or near-infrared frequencies (usually 600-1100nm).

1.4.2 OPC

The introduction of OPCs, which occurred in the mid-20th century, accelerated in the 1960s with the invention of the laser. The initial focus of particle counting in cleanrooms [17, 18, 19] was later extended to air quality assessment and industrial hygiene [20]. In this category of instruments, a light source, typically a focused incandescent lamp or laser source, is used to sample a small volume of fluid.

It is important to avoid the simultaneous presence of more than one particle in the same volume to avoid the generation of bias. Commercial instruments work with a maximum concentration of one million particles/liter. For higher concentrations a dilution of the sample is mandatory. Although this dilution reduces the accuracy of the concentration determination. In practical applications, the particle size distribution is determined by comparing the light

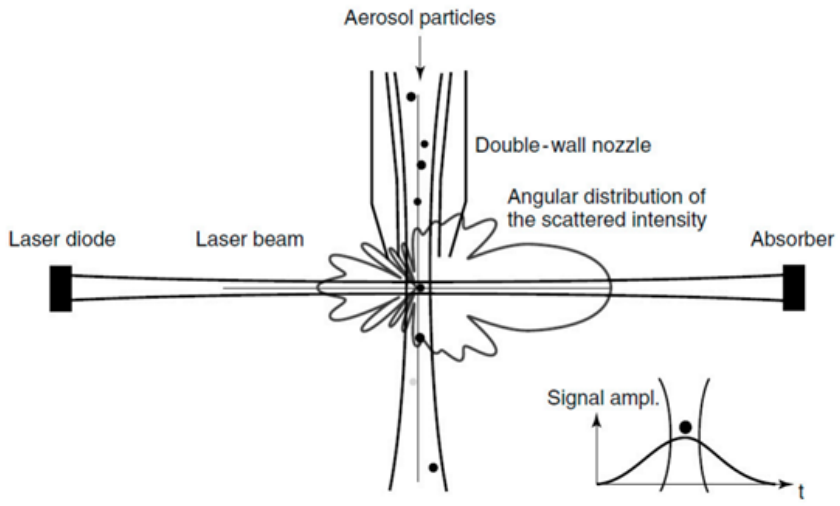

Figure 1.4: Generic scheme of an OPC: the particle crossing the illumination zone (viewing volume) generates a diffraction pattern at a 360° angle. The corresponding impulse recorded by the photodiode is shown in the inset; the intensity of the signal depends on the particle size, while its width is correlated to the viewing volume.

intensities generated by the passage of each individual particle through a small illuminated area, with a standard curve calibrated using a series of sometimes mono-dispersed particles or at least particles of known size.
To assess particle concentration, the sampled air volume is measured simultaneously.
The most common configuration involves perpendicular scattering geometry because the perpendicular positioning of the photodetector ($\Theta = 90°$) limits the effects of stray light within the device.
Briefly, in an aerosol laser spectrometer, an air sample is drawn into a narrow inlet that limits stray particles; a collimator generates a laser curtain perpendicular to the inlet stream. When infrared laser light illuminates the particles in the air sample, a scattering signal is produced and detected at right angles by a photodiode (see Figure 1.4).
In accordance with Mie's theory, each measured pulse height is related to the particle size. A portion of the light scattered at a certain angle is collected by a photodiode. The amplitude of the detected signal is compared

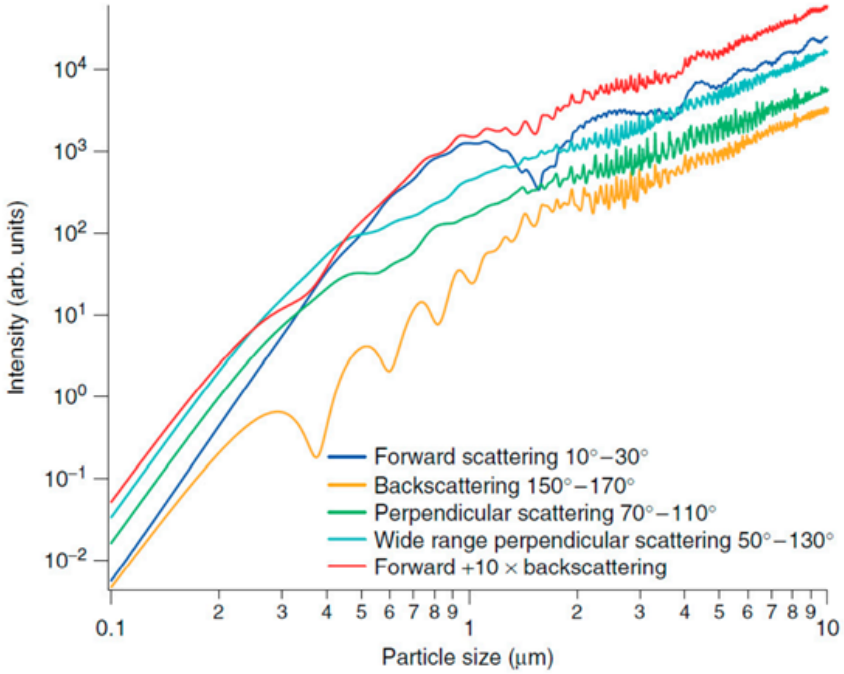

Figure 1.5: Calibration curves calculated for different scattering angles and integration intervals for polystyrene latex: in the case of front-to-back scattering, the relationship between size and scattering intensity in some size intervals, namely the 0.4-1μm interval for backscattering and the 1-3μm interval for front scattering, is not uniform. In the case of perpendicular scattering, shorter oscillations are observed in the range of 2-5μm; the latter geometry is preferred both because of its size distribution and because it has less dependence on the refractive index of the particles

with the standard calibration curve obtained from the particle sample. As an example, the calibration curves calculated by Aladar Czitrovszky [21] using Mie theory for different scattering and integration angles are shown in Figure 1.5. From these curves, the relationship between size and scattering intensity in certain size ranges is shown to be non-uniform. The output of an OPC is a time-monitored electrical signal consisting of a sequence of pulses; the intensity of each pulse represents the light scattered by a particle passing through the OPC and is related to its size by a calibration curve. Particles are counted and considering the air flowing through the OPC, the concentration of particles in the air and their size can be determined.

1.5 LCPMS characterization and calibration

In recent years, several scientific works have contributed to evaluating the performance of different LCPMS devices. The growing number of these types of sensors and the various evaluation techniques proposed for their parameters have raised questions about how to evaluate and define their performance.
It was not until two years ago, in 2018, that the EPA finally defined the characteristic parameters for this class of devices. Since then, several articles have reported on the calibration and characterization of LCPMS using different types of setups, including laboratory conditions, partially controlled conditions, and field deployment conditions. In the following section, a review of some of these relevant works is provided.

1.5.1 Laboratory characterization

Deploying affordable PM sensors requires a great deal of effort to ensure their data reliability. These sensors must be calibrated with reference instruments and fully characterized under a variety of environmental conditions. Consequently, the development of characterization chambers in the laboratory is critical to facilitating realistic testing in a controlled environment. The characterization phase in the laboratory, under controlled environmental conditions and pollution levels, allows for the evaluation of the performance of low-cost sensors before their deployment in the field and the assessment of possible differences in their responses within the same family of LCPMS, the latter being of particular relevance to their application in sensor networks [22].
In general, an aerosol chamber consists of three main sections: a test chamber (TC), which is isolated from the external environment and equipped with a PMreference instrument and humidity (RH) and temperature controls; a purified air system, which is required to provide clean reference air into the TC; and a PMgenerator that ensures a controllable PMconcentration within the test chamber. A general schematic of an aerosol chamber for PMmeasurement is shown in Figure 1.6. In recent years, several types of test

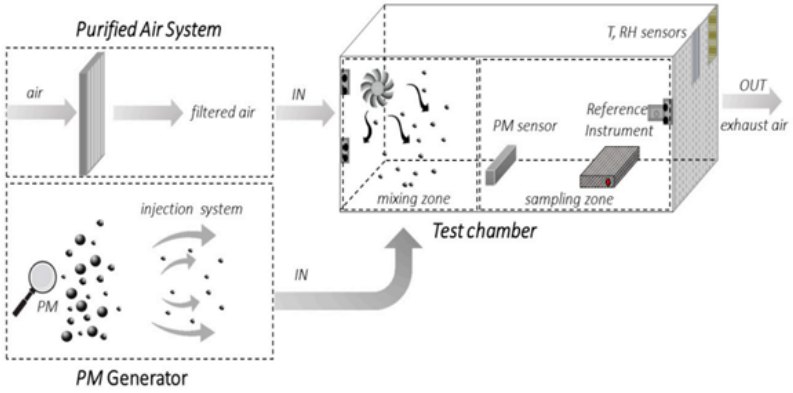

Figure 1.6: A schematic of the PMcharacterization system: PMgenerator, purified air system, and test chamber with PMsensors, Reference Instruments and T, RH sensors.

chambers have been proposed. One of the first test chambers was fabricated by Yang Wang in 2015 [23]. A custom-built acrylic glass chamber was assembled ($58 \times 58 \times 28 cm^3$, chamber volume of 94.19 L) with its edges sealed using rubber strips to prevent PMleakage. The authors placed three LCPMSs (Samyoung DSM501A, Shinyei PPD42NS, Sharp GP2Y1010AU0F) on each vertical wall to minimize spatial differences in PMconcentration. Particles were produced from aqueous solutions of NaCl, sucrose (C12H22O11), and NH4NO3, and atomized by an aerosol generator (Model 3076, TSI Inc.) and incense burning (Agarbathi sandalwood cones, Cycle brand).
The particles were dried, sent to the test chamber, and suspended through fans. The apparatus was equipped with a probe sensor and thermocouple to monitor temperature and humidity during the test. A SidePak-TSI Inc. (St. Paul, MN, USA), a scanning mobility particle analyzer (SMPS-TSI Inc.), and an AirAssureTM $PM_{2.5}$(TSI Inc.) were used as reference instruments and located outside the test chamber. All three LCPM sensors showed high linearity concerning the SidePak with incense particles up to a 0-300$\mu g/m^3$concentration range. Specifically, the authors obtained a correlation coefficient $R^2$of 0.9525 for Shinyei PPD42NS, 0.9755 for Samyoung DSM501A, and 0.9746 for Sharp GP2Y1010AU0F. In addition, this work showed how humidity and particle size/composition affected sensor perfor-

mance, which did not happen with temperature.
Austin et al. constructed a small airtight box ($6 \times 21 \times 8cm^3$, total volume 1L), which was further reduced by placing a fixed baffle along with the box [24]. Four LCPM sensors (Shinyei PPD42NS) were placed in this box. Monodisperse polystyrene balls and polydisperse powder (ASHRAE test powder #1) were used as particle sources and were sprayed before entering the chamber. Filtered dry air was used as a baseline for measurements. The particulate aerosol was injected with steel tubes into the first chamber, where the particulate was suspended by four blower fans. Then, the particulate was sucked towards the sensors using the internal pump of the TSI APS (Aerodynamic Particle Sizer), the reference instrument, in series with the Shinyei sensor chamber. The aerosol was generated until the particulate concentration reached a specific value. Then, aerosol injection ceased along with particle decay measured using both the APS and the sensors in series. This comparison showed that the accuracy of the Shinyei sensors compared to the APS can be as high as 0.99 $R^2$to monodispersed aerosols in a concentration range of 0-50$\mu g/m^3$. The authors concluded that the Shinyei PPD42NS sensors have adequate sensitivity for monodisperse aerosols, but in cases of polydisperse aerosols with unknown composition, mass conversion was only possible using a gravimetric method.
Thomas Peters et al [25] developed a more complex system to evaluate low-cost sensor performance in the presence of high particle concentrations relative to professional applications (up to 6500$\mu g/m^3$). In the experimental setup a single chamber was divided by a perforated plate into two distinct zones: a mixing zone ($64 \times 64 \times 66cm^3$) and a sampling zone ($53 \times 64 \times 66cm^3$, V 224L). The perforated plate (600 holes with a diameter of 0.6 cm) ensured uniform particle distribution. Zero air (clean air through HEPA filters) diluted the generated aerosol. Particles were placed under laminar flow (0.01m/s), and three DC1700 sensors, two Sharp sensors (Sharp GP and Sharp DN), and a pDR-1500 photometer were placed in the sampling zone. Laboratory analytical instruments located outside the chamber included a condensation particle counter (CPC; 3007, TSI Inc., particle diameter $\leq$ 0.3μm) and an aerodynamic particle analyzer (APS; 3321, TSI Inc., parti-

cle diameter $\geq 1\mu m$). In addition, a sequential mobility particle analyzer (SMPS-C 5.402, GRIMM) ensured that particle generation was monodispersed. The authors tested the four types of particle types (Arizona dust, salt, diesel exhaust, and welding fumes), which were generated in different. ways. In detail, salt droplets were obtained through a Carefusion nebulizer, a fluidized bed generator (3400A, TSI Inc.) produced an Arizona dust aerosol, diesel exhaust fumes were derived from a diesel generator, and welding fumes were extracted from a welding apparatus. The LCPM compared photometer (pDR-1500) showed a high correlation coefficient ($R^2 > 0.97$) and high accuracy ($< 8\%$).

Papapostolou et al. developed a test chamber shown in Figure 1.7 [18]. This chamber highlights the possibility of introducing several gases at the same time; the chamber also monitors the temperature, pressure, and relative humidity and uses a constant concentration of PM. Dry, particle-free systems are used to generate the reference air. Specifically, the equipment consists of two chambers: the outer and inner chambers. The first is a rectangular stainless steel chamber (volume approximately 1300L) with LCPM sensors and reference instruments (GRIMM (EC180-FEM), TSI (model 3321-BAT) and TSI (model 3091-BAT). The inner chamber is a Teflon-coated stainless steel cylinder (volume 110L) used for monitoring gas sensors. This configuration allows direct comparison between LCPM sensors and reference instruments during measurement. there are also two different aerosol generators to generate ultrafine/fine particles (model AGK 2000, PALAS, Karlsruhe, Germany) and fine/coarse particles (model SAG 410/U, TOPAS, Dresden, Germany). The authors conducted experiments to demonstrate the system's ability to produce stable and reproducible gas and aerosol atmospheres over a wide range of temperature (T) and relative humidity (RH) conditions.

Subsequently, Hapidin's group also proposes a characterization system [26]. The authors adopted an exponential particle concentration decay to evaluate three PM sensors (Sharp GP2Y1010AU0F, Winsen ZH03A, and Novafitness SDS011), as previously seen in Wang's work [17]. The authors noted that, compared to other test methods using constant particle concentrations, this concentration condition can greatly reduce the test time [18, 24, 25],

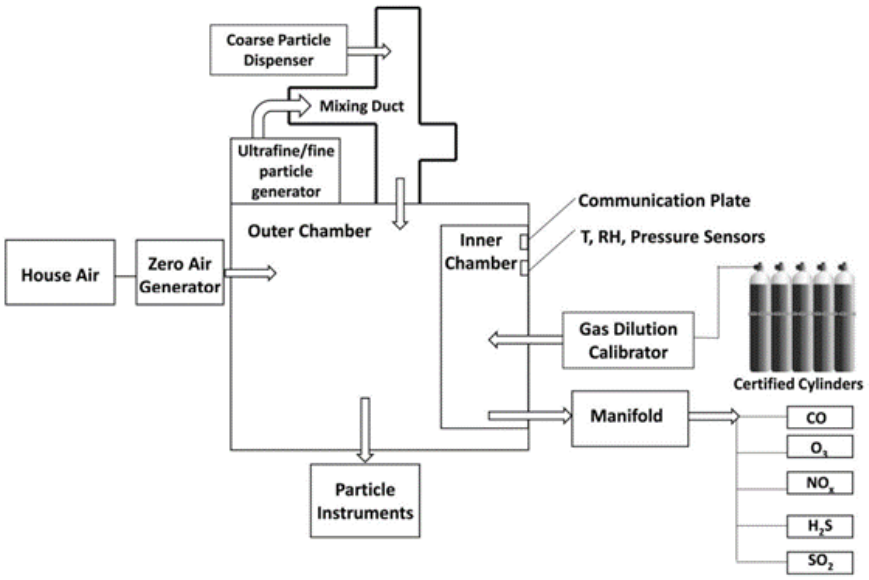

Figure 1.7: Schematic of the chamber system developed by Papapostolu et al. (2017).

as this device has an additional airflow outlet to accelerate the decay of PMconcentration.

The aerosol chamber was custom-built from acrylic material (with a volume of 70.53L). In the test chamber, two reference instruments (a CPC-TSI, model 3025A and a factory-calibrated particle sensor, Honeywell, model HPMA115S0-XXX) were placed next to three LCPM (Sharp GP2Y1010AU0F, Winsen ZH03A, and Novafitness SDS011). Aerosol was generated by burning incense and sent to the test chamber until a concentration of $1000\mu g/m^3$(the detection limit of HPMA) was reached. In this system, a silica gel pump and HEPA filters ensured dry and clean incoming airflow. The results showed good linearity with the HPMA reference monitor, with R^2values of 0.999 for the Novafitness SDS011 at low particle concentration (0-$400\mu g/m^3$). In addition, the Winsen ZH03A sensor and Novafitness SDS011 showed coefficients of variation less than 10%, which is within the accuracy of precision established by EPA standards.

Kim et al [27], used two types of test systems. One used a mixing chamber (50L), where particles were mixed with clean air, and the overall airflow

velocity was carefully adjusted to ensure proper operation of the dust sensor. In the second system, an exponentially decaying particle concentration was obtained in a low air velocity duct. Particles generated by an atomizer were first introduced into a particle mixing chamber until the particle concentration reached the appropriate level. Then, the particle inlet was closed and clean air was supplied to the particle mixing chamber. A 5% potassium chloride (KCl) solution was used to generate particles through an atomizer for both test systems. The reference instrument for measuring size distributions was a Grimm 1.209 dust monitor (model 1.209, Grimm Aerosol Technik Company, Ainring, Germany). A large-scale comparison work was then performed. The authors tested about 264 LCPM sensors and classified them into four different groups (classes 1, 2, 3 and 4) based on their performance compared to the reference instrument. Most of the sensors showed very good linearity (slope of concentration measurement data) with the reference data. Approximately one-quarter of the tested sensors met the class 1 acceptance limit. However, accurate PM_{10}measurements were rarely obtained, probably due to the difficulty of transporting large particles to the detection areas.
Based on Papapostolu's measurement method, Omidvarborna et al. designed an environmental pollution chamber to test LCPMS performance under a controlled temperature and relative humidity (RH). Different types of particles and concentrations of polluting gases could be produced in this chamber [28]. The authors constructed the test chamber ($50 \times 50 \times 50cm^3$5, V 125L) from Teflon-sprayed acrylic sheets insulated by $100nm$ polystyrene. The sheets were used to minimize surface reactions for gas and aerosol experiments. The inner edges of the chamber were sealed with rubber strips to prevent leakage. The environmental chamber was connected to a humidifier/dehumidifier system, a heat pump, a particulate matter generator, a supply of gaseous pollutants O_3, NO, NO_2, SO_2, hydrogen sulfide H_2S, and reference measurement instruments (a Vaisala HMT120 a temperature/RH sensor and an optical particle counter, Grimm EDM 107). This chamber was able to reproduce outdoor and indoor environmental conditions (a temperature range of 5 to 40 $°C$ and a RH of 10% to 90%) and stable pollutant concentrations. After comparing the results obtained with the tempera-

ture/RH sensors and the Honeywell HPMA115S0 particulate sensor with those obtained from the reference instrumentation, the authors found a good correlation, with R^2values above 0.96, 0.99, and 0.97 for temperature, RH, and $PM_{2.5}$, respectively. The results, according to the authors, showed that this chamber could be particularly attractive because of its affordable cost, small size, lightweight, and ease of operation. This chamber generated similar environments and pollutant concentrations to evaluate the performance of LCPMS under various conditions.

In recent work, Bulot et al. applied exponential particle concentration decay with median peak concentrations of $PM_{2.5}< 40\mu g/m^3$using two different pollution sources to test 40 LCPM sensors (produced by five manufacturers) [29]. $PM$from the combustion of incense sticks was sent to the chamber through dry, filtered air (flow rate of 5L/min) using the MFC 1179A, while $PM$from the combustion of candles was sent into the chamber wall using an angled chimney. This chimney was kept sealed throughout the remaining time. The authors used a $1m^3$ Perspex/stainless steel chamber framed by aluminium profiles. Fans ensured air mixing within the chamber. A temperature-controlled walk-in room (Viessmann A/S; setpoint between 25.9 and 28.7 $°C$) contained the chamber, and RH was varied between 5% and 90% within the chamber by the modulated introduction of filtered air, dry air, or humidification via a Nafion MFC membrane (MKS type 1179A 20 L/min plus type 1579a 100 L/min). The chamber pressure was allowed to reach equilibrium before starting each test. The authors characterized eight different LCPMS models for each of five different manufacturers: the Honeywell HPMA115S0, Alphasense OPC-R1, Novafitness SDS018, Sensirion SPS030, and Plantower PMS5003. Finally, sensor performance was evaluated through reference measurements obtained from a DustTrak DRX 8533 Desktop device (TSI Inc., Shoreview, MN, USA), an Optical Particle Sizer OPS 3330 (TSI Inc.), and an Aerasense Nanotracer (Oxility BV, Best, The Netherlands). Using this test system, the authors highlighted the different behaviours of the tested LCPMS under various PM types and their coefficients of variation based on their responses to peaks or stable particle concentrations. The results allowed the authors to compare the performance of different LCPMS

models. The coefficient of variation reached higher values when comparing responses to peak values than when comparing stable particulate concentrations for all sensors. Alphasense OPC-R1 produced the highest coefficients of variation under both peak and stable conditions. However, all sensors showed better performance when it comes to candle-generated PM. In particular, the Sensirion SPS030 and Plantower PMS5003 achieved similar scores regardless of the rate of change in concentration (peak or stable concentrations). The other three sensor models showed lower scores for stable concentrations, indicating better performance in peak concentration regimes. The authors concluded that the Sensirion SPS030 achieved the lowest coefficients of variation among all sensor models, regardless of the test scenario.

In all of the above work, the generation of particles and their injection into a test chamber are critical issues. To create a uniform environment in terms of concentration and composition, controlled systems are generally used. Some authors use fully automated aerosol generators to achieve stable and reproducible particle environments [18, 24]. In one case, an aerosol generator (TOPAS SAG 410) was coupled with an aerosol wind tunnel [30]. In this study, particulate matter was maintained in a low wind speed flow (less than 0.5 m/s) to reproduce typical values for most work environments. The wind tunnel was $1.22 \times 1.22 \times 6m^3$ with the area of the sampling zone having a length of about 3m and the airflow through the wind tunnel was generated by four fans. This work showed that fan speed directly affected particle concentrations: the higher the fan speed, the greater the chance that a particle would hit the chamber walls, leading to lower aerosol concentrations.

Other authors have suggested homemade systems to obtain $PM$from more readily accessible materials. In Ristovski's laboratory, cigarette and e-cigarette smoke was studied as a source of indoor particulate matter [31, 32]. In other work, various indoor air fresheners such as aroma diffusers, Armenian paper, incense, candles, and instant or automatic sprays [33]. Incense burning is a particularly useful source of particulate matter because it produces a monodisperse aerosol suitable for representing $PM_{2.5}$[34, 35].

In addition to particulate matter production, several methods have been proposed to introduce PMinto the chamber test. Zamora's group used three

different methods depending on the source of PM. For incense, a stick was lit and placed inside a holder until the required concentration was reached. Then, the stick was removed and a decrease in concentration was observed; talc was also studied after being dispersed with filtered air and injected into the test chamber. Sodium chloride (NaCl) and oleic acid were also used in a collision nebulizer (CH Technologies, Westwood, NJ, USA). In this case, filtered air flowed through the nebulizer, which was filled with a solution of NaCl water or pure oleic acid until the desired concentration of NaCl or oleic acid was reached. then the incoming airflow was turned off [36].
Several authors have also proposed the use of commercial pressurized metered-dose inhalers (pMDIs), such as Atrovent and Ventolin. By pressing the bottom of the containers of such inhalers, a well-defined dose of the drug is released. The container contains the powdered drug dispersed in a liquid propellant with other additives [37]. The authors estimated the particle size using the MMAD (Mass Median Aerodynamic Diameter): when the bottom is pressed, a mixture of drug and aerosol is formed, whose particle diameter depends on the evaporation of the propellant and the distance from the exit. At the exit, the particle diameter is 30-40μm including the aerosol-cloud surrounding the particles, while at a distance of about 10 cm from the valve, the diameter decreases to 2-3μm. To use this system for particle generation, several boundary conditions need to be evaluated in the overall context of the experiment. Rui Zhang studied the effect of environmental conditions (temperature and humidity), flow rate, and device temperature on the size of the particle size emitted through pMDI[38].

1.5.2 Field characterization

Field characterization of LCPMS is a critical task, even if preceded by laboratory characterization. Even with the best available technologies, one of the main problems is to replicate real-world conditions, since the diversity of particulate physicochemical compositions can only be definitively assessed in the field. For field characterization, after performing laboratory tests as mentioned above, the authors in [36] tested their sensors in an indoor environ-

ment (a 1000 ft^2 apartment; specifically, the campaign monitored a kitchen) using a pDR-1200 (TEOM) as a reference. For the outdoor measurements, the LCPMS network was placed at the University of Baltimore MDE at a major intersection at a height of 5 m; at this location, approximately 50,000 vehicles pass by each day. Site measurements were obtained in the summers of 2016 and 2017 and applied both a gravimetric and a BAM (FEM) system, resulting in a linear correlation coefficient $R^2$of 0.92 with the reference PMmeasurements.

In [39], Plantower sensors were tested at a major roadway intersection near Salt Lake City. The sensors used a sampling rate of 1 minute and, depending on whether they were compared to a FEM or FRM, the data were averaged over 1 or 24 hours. Results showed that linear correlation coefficients with the FRM varied widely by season, reaching a minimum in spring (0.185 for PMS1003 and 0.419 for PMS5003), while the highest correlation was observed in winter, where they rose to 0.972 and 0.971, respectively. In addition, the authors indicated significant drift after 3 months when using pms1003. The authors in [40] developed a 1-year comparison of four different LCPMSs (Alphasense OPC-N2, Plantower 5003, Plantower 7003, and Honeywell HPMA115S0), which were all located near two schools in Southampton, against a UK reference station (AURN). The closest AURN $PM_{2.5}$monitoring station was located in Portsmouth, 40 km to the east, and was equipped with FDMS 8500 and TEOM 1400ab Ambient Particulate Monitor, which was reported hourly $PM_{2.5}$concentrations along with volatile and non-volatile $PM_{2.5}$. The comparison shows that the two Plantower sensors showed linear correlation coefficients (R^2) always greater than 0.8, while for the OPC-N2, the $R^2$was always less than 0.7.

In [41], a six-month measurement campaign with four LCPMSs (SDS011, ZH03A, PMS7003, and OPCN2) was performed at the Meteorological Observatory of the Department of Climatology and Atmospheric Protection at the University of Wrocław. The reference systems provided by this site were TEOMs. In this work, the Plantower again showed the best linear correlation compared to the reference instrument, achieving an $R^2$of 0.93 when its raw data were averaged over 24 hours. The authors analyzed how the correla-

tion coefficient varies by measurement interval for Novasense and Plantower, dividing the latter into three zones: (1) $<20\mu g/m^3$(2) 20-60$\mu g/m^3$and (3) $>60\mu g/m^3$. Surprisingly, at very low concentrations and in the first zone, no sensor was able to achieve a linear correlation coefficient of 0.6 (with both 15-minute and 1-hour averages).

In [42], Alvarado et al. attempted to characterize a low-cost dust sensor (Sharp GP2Y10) unusually. The authors installed two sensors on two different UAVs (on the fixed and rotating wings), where the air intake and exhaust were modified to achieve controlled flow within the sensor. Bench tests were conducted using incense combustion, and nonlinear regression was used to calibrate and evaluate the potential correlation between the sensors and a commercial industrial analyzer (DustTrack 8520) at very high concentrations (0-120$\mu g/m^3$), resulting in relative errors ranging from 0 to 120$\mu g/m^3$), producing relative errors ranging from 12% to 22%. After careful analysis to filter out the noise produced by the switching of the UAV's electric motors, the authors performed tests under controlled operating conditions to reconstruct the 3D concentration fields of the particulate matter. One of these tests included pumping talc with a garden blower, so the sensors were recalibrated to handle the composition of these new particles. The authors concluded that the integration of air quality sensors and autopilot data is potentially feasible and would allow the determination of the distribution of airborne particulate matter over time and space. However, the authors recommended the use of new optical sensors with higher sensitivity and calibrations that can rule out cross-contamination for more realistic concentration scenarios.

AQ-SPEC [43] provides evaluations for LCPMS operating in the field, in addition to those they provide for laboratory setup. In the first case, low-cost sensors are compared to FRM or FEM monitoring instruments, which are typically used to detect pollutants for regulatory and legislative purposes. Specifically, for PMdetection, the research centre uses a GRIMM EDM180, which is an optical-based PMmeter (like most LCPMS); it is considered a FEM by the EPA and provides real-time particulate concentration measurements. They also rely on two MET ONE 1020s (one for $PM_{2.5}$and one for PM_{10}), which are beta-ray attenuators that provide hourly averages of air-

borne particle concentration. For field evaluations, AQ-SPEC researchers refer to a rigorous protocol, in which, after verifying the correct match between the "bench" test and the documentation (power specifications, data acquisition method evaluation), the LCP data acquisition method), the LCPMS are placed in the monitoring station for 30-60 days. The sensors are checked for operation and recording every week [44]. The tests, reported in [45] show (1) sensor image, (2) sensor manufacturer and model, (3) price, (4) pollutant tested ($PM_{2.5}$, PM_{10}, etc.), (5) coefficient of determination R^2in the field, (6) coefficient of determination R^2in the laboratory, and (7) a summary report providing the linkage of each specific sensor. Their efforts, along with those of other organizations such as EPA [46], to build a crystal-clear picture of the actual performance of PM and LCPMS meters in both the field and laboratory, using reference instruments, is critical for the general public to understand the real-world capabilities of these instruments and for professionals to choose (low-cost) instruments for environmental monitoring. More significantly, their work supports other researchers in implementing test chambers for environmental sensors and developing a measurement protocol for field assessments.
All articles indicate fundamental differences between laboratory and field testing. In a field characterization, facilities can record data for several months with instruments left unattended for several days or weeks. The long-term results of these characterizations depend on their correlation with a reference instrument, but accuracy is difficult to estimate because it depends on the relative position between the LCPMS and the reference instrument.

1.6 LCPMS performance literary review

In this section, we present the performance exhibited by the LCPMS that has been studied in the scientific literature. The sensors are classified by several characteristic and hallmark parameters, mostly derived from EPA definitions. Some of the most significant parameters are summarized in Table 1.4, where

the columns refer to the quality indicators that have been reported by the authors to evaluate their performance of theirs against a reference instrument, which is shown in the last column:

- **Accuracy**
  A measure of the overall agreement of a measurement with a known value (i.e., an accepted reference value). Along with bias, the R^2value of a regression model's predictions, listed here, is a generally accepted measure of the potential of the calibrated instrument accuracy. Its value can range from $-\inf$ to 1.

- **Precision**
  A measure of the agreement between repeated measurements of the same property under identical or substantially similar conditions, calculated as a range or standard deviation.

- **Bias**
  The systematic or persistent bias in a measurement process that causes errors in one direction.

- **Completeness**
  A measure of the amount of valid data that must be obtained from a measurement system.

- **Detection limit**
  The lowest level of analyte that can be reliably identified.

- **Measurement range**
  The minimum and maximum concentration range that the instrument is capable of measuring.

When different reference instruments are used, a direct comparison of reported performance levels requires caution. Some work compares the concentration estimates of low-cost devices with those of officially recognized measurement methods by government agencies, i.e., those based on several different measurement principles such as FRM and FEM. A relevant example

may be in the work of Sayahi et al. [39], who tested two LCPMSs manufactured by Plantower with a gravimetric FRM and a TEOM (FEM) for 320 days. Due to the long sampling time of FRM and FEM, the comparison was made by considering the average of the measurement periods which became comparable to that of the reference instruments. In other surveys, LCPMSs were compared to certified OPCs used as reference instruments. These comparisons were primarily implemented under laboratory conditions with controlled setups, although several articles report on the performance of field use. The high temporal resolution of OPCs, which is comparable to that of LCPMSs, provides more accurate information about the quality of measurements from low-cost devices. For example, Feinberg et al [47] compared LCPMS performance with a Grimm 180 EDM, and Han et al [48] used a Grimm 11R as a certified instrument to compare devices over a 12-day duration. Several articles rely on both types of reference instruments to obtain an even broader comparison.

Table 1.4: The most meaningful LCPMS parameters. The columns report the quality parameters used to evaluate performance compared to a reference instrument, which is reported in the last column.

	Ref	Test Year	PM Class	Accuracy R^2 * Tested in alaboratory setup	Bias $\mu g/m^3$	Completeness	Detection Limit $\mu g/m^3$	Measurement Range $\mu g/m^3$	Precision %	Reference Instrument
Plantower PMS A003	[35]	2018	2.5	0.91				0-49	12	PDR-1200
Plantower PMS 1003	[39]	2019	10	0.91						Gravimetric FRM
Plantower PMS 5003	[39]	2019	10	0.7						Gravimetric FRM
Plantower PMS 1003	[39]	2019	2.5	0.88		56.9%				Gravimetric FRM
Plantower PMS 5003	[39]	2019	2.5	0.89		11.6%				PartisolTM 2025i Sequential Air Sampler)
Plantower PMS 7003	[17]	2019	2.5	0.96				16-75	16	TEOM SEMC/GRIMM 1.108
Plantower PMS 7003	[17]	2019	10	0.97				16-75	14	TEOM SEMC/GRIMM 1.109
Novasense SDS011	[19]	2018	2.5	0.96				3-79		TSI DustTrak DRX
Novasense SDS012	[19]	2018	10	0.91				3-90		TSI DustTrak DRX
Alphasense OPCN2	[49]	2018	2.5	0.9				0-300		Grimm1.108
Alphasense OPCN2	[49]	2018	10	0.84				0-350		Grimm1.108
Alphasense OPCN2	[51]	2019	2.5	0.50				0-35		TEOM AURN
Honeywell HPMA115S0	[51]	2019	2.5	0.77				0-35		TEOM AURN
Plantower PMS 5003	[51]	2019	2.5	0.76				0-35		TEOM AURN
Plantower PMS 7003	[51]	2019	2.5	0.73				0-35		TEOM AURN
ZH03A (Winsen)	[41]	2018	2.5	0.81	3.27			0-120	25	TEOM 1400a
Alphasense OPCN2	[41]	2018	2.5	0.61	8.36			0-120	37	TEOM 1400a
Plantower PMS 7003	[41]	2018	2.5	0.89	3.36			0-120	11	TEOM 1400a
Novasense SDS011	[41]	2018	2.5	0.9	4.76			0-120	12	TEOM 1400a
Alphasense OPCN2	[47]	2018	2.5	0.2		82.00%				grimm edm 180
Alphasense OPCN2	[47]	2018	10	0.46		82.00%				grimm edm 18
Shinyei PMS-SYS-1	[47]	2018	2.5	0.52		92.00%				grimm edm 180
Alphasense OPCN2	[50]	2017	10	0.81	0.32			0-250		Bam 1020
Alphasense OPCN2	[50]	2017	10	0.84	2.83					grimm11R
Alphasense OPCN2	[50]	2017	2.5	0.43	1.92					grimm11R
Alphasense OPCN2	[40]	2019	2.5	0.45				0-100		TEOM AURN
Plantower PMS 5003	[40]	2019	2.5	0.7				0-100		TEOM AURN
Plantower PMS 7003	[40]	2019	2.5	0.77				0-100		TEOM AURN
Alphasense OPCN2	[52]	2019	2.5	0.81				0-146		teom
Honeywell HPMA115S0	[53]	2019	2.5	0.58				0-72.9		grimm edm 180
Honeywell HPMA115S0	[26]	2019	2.5	0.99						TSI-3025A
Novasense SDS011	[26]	2019	2.5	0.90 *						TSI-3025A
ZH03A (Winsen)	[26]	2019	2.5	0.98						TSI-3025A
sharp GP2y	[26]	2019	2.5	0.96						TSI-3025A
Alphasense OPCN2	[54]	2018	2.5	0.78				0-70		Palas Fidas 200
PPD42NS	[55]	2018	2.5	0.8			9.1	0-500		TSI DustTrak
PPD20V	[55]	2018	2.5	0.98			4.6	0-500		TSI DustTrak
PPD60PV [138]	[55]	2018	2.5	0.87			29	0-500		TSI DustTrak
sharp GPD2y1010AU0F	[52]	2018	2.5	0.99				0-8000		TSI AM510 â€˜Sidepakâ€™
sharp GPD2y1010AU0F	[51]	2017	2.5	0.99 *			10.93	0-1000		Alphasense OPC-N2
sharp GPD2y1010AU0F	[23]	2015	2.5	0.99 *			26.9	0-5000		TSI AM510 â€˜Sidepakâ€™
Shinyei PPD42NS	[23]	2015	2.5	0.95			6.44	0-300		TSI SidePak
Samyoung DSM501A	[23]	2015	2.5	0.98			11.4	0-300		TSI SidePak
sharp GPD2y1010AU0	[55]	2012	10	0.99				0-3000		TSI AM510 â€˜Sidepakâ€™
sharp GPD2y1010AU0F	[42]	2015	2.5	0.98 *				0-140		Dusttrak 8520
sharp GPD2y1010AU0F	[42]	2015	10	0.91 *				0-120		Dusttrak 8520
sharp GPD2y1010AU0F	[25]	2016	2.5	0.95				30-6300	<6%	SMPS/CPC(GRIMM)-APS
Sensirion SPS30	[52]	2019	2.5	0.83 *						Grimm1.108
Alphasense OPC-N2	[54]	2016	2.5	0.99 *				10-10.000	4.2-16%	SMPS/CPC(GRIMM)-APS 3321

For example, Crilley et al [49], in addition to a TEOM (FEM) used two certified OPCs (a TSI3330 and a Grimm Pas1.108) as reference instruments, and Mukherjee et al [50] used a BAM- 1020 (FEM) and a Grimm-11R OPC.

Alphasense N2

As shown in Table 1.4, this is the most commonly tested PM sensor in the scientific community. Of the low-cost sensors, this is one of the most expensive and is capable of measuring PM_1, $PM_{2.5}$, and PM_{10}concentrations because it can count particles with sizes between 0.3 and 25 μm, dividing this range into 16 bins of size. Crilley et al. tested this sensor through field evaluations against two different reference systems over two weeks [49]. The two reference systems were a Grimm PAS-1.108, which is a certified optical particle counter, and a TEOM, which is an EPA-recognized FEM. In this paper, the authors discuss issues related to moisture interference, showing that for all sampling points obtained over the two weeks, the R^2values reached 0.72 for both the Grimm and TEOM when measuring $PM_{2.5}$, with 0.67 for the TEOM and 0.68 for the Grimm when measuring PM_{10}. However, these correlation coefficients increased significantly, exceeding 0.8 in all cases, when only sampling points with measured relative humidity below 85% were considered. This confirms that humidity is one of the most important interferents for this type of device.

Johnston et al., as part of an IoT project, aimed to create an air quality monitor using an LCPMS. The authors tested various sensors in the field, specifically around two schools, for two weeks in June 2018 [51]. The authors compared their data with data from AURN stations, which is the official reference method used in the UK. For $PM_{2.5}$measurements, Alphasense N2 obtained the worst $R^2$of 0.5, compared to values above 0.7 measured on other LCPMS, such as Plantower PMS 5003, Plantower PMS 7003, and Honeywell HPMA115S0.

In addition, Badura et al [41] tested this LCPMS in the field along with three other devices, comparing them to a TEOM during a 6-month measurement campaign. The novelty of this work is the comparison between the LCPMS and the reference instrument using different averaging times (1 min, 15 min,

1 h, and 24 h). As expected, better results were obtained for all devices when increasing the sampling time. As in [47], N2 provided the worst results, achieving a maximum $R^2$of 0.69.
In [47], Feinberg et al. field-tested several environmental sensors, not only for PMbut also for gases, over 6 months between late 2017 and early 2018. The authors used a Grimm EDM180 as a reference for PM, with a sampling time of 1 min. In this work, the authors obtained the worst overall result for Alphasense N2, obtaining only 0.2 for the R^2correlation index for $PM_{2.5}$and 0.46 for PM_{10}. Mukherjee et al., in a paper describing a 3-month field campaign, estimated the effects of wind on particulate measurements using these devices [50]. The authors used two different reference devices, one with the same physical principles as the LCPMS, the Grimm-11R, and the other with a different physical principle, the BAM-1020 (FEM). As a result, they obtained an $R^2$of 0.84 for PM_{10}, indicating good performance, but the R^2dropped dramatically to 0.43 in the best case, compared to the Grimm, for $PM_{2.5}$.
Bulot et al. tested four LCPMS sensors, including an Alphasense N2, for two months in two schools in the United Kingdom, using the official government system as a reference (AURN) [29]. Among the sensors tested, the N2 again offered the worst performance for $PM_{2.5}$with a maximum correlation coefficient of 0.45. This value is very low compared to that obtained with Plantower, which exceeded 0.7 for R^2. In [52], Feinberg et al. compared 20 different units of Alphasense OPC-N2 with a TEOM for about 6 months. In this work, the R^2values of the various units were very scattered, reaching a maximum of 0.81 but below 0.5 for most units.
Di Antonio et al. calibrated N2 in the field using a Palas Fidas 200 as a reference. This reference device is a certified instrument based on optical light scattering [53]. The authors showed that, after calibration, the R^2increased from a value of 0.34 to a much more acceptable value of 0.78 by correcting the data for recorded relative humidity. This again confirmed that this device suffers under particularly high humidity levels.
In [[54], Susan et al. calibrated their sensor in a laboratory rather than in the field (i.e., they used a controlled environment with a particulate concen-

tration of up to 10,000 $\mu g/m^3$). This value is much larger than the dust regimes found in the field, which barely exceed $100\mu g/m^3$. In this case, the R^2value reached 0.99 for both PM10 and PM2.5. The authors concluded that at high concentrations and under controlled conditions, the performance of this device is excellent.
Finally, despite its price (which is the highest among LCPMSs), the N2 provides the worst performance in the field, as indicated in the literature. The N2 is one of the first LCPM sensors to appear on the market, and it came with a detailed datasheet reporting on relevant lab tests. Its strengths are its hardware and firmware, which allow it to collect detailed information not only on PM measurements but also on particle bin counts and their specificity for $PM_{2.5}$. However, N2 performs poorly in low concentrations and is one of the bulkier devices.

Plantower family
Plantower (models PMS1003, PMS3003, PMS5003, PMS7003, and PMS-A003) offers a wide variety of sensors at a lower price point than other manufacturers.
Zamora et al. tested the PMS-A003 both in the laboratory in an indoor environment and in the field, comparing the data with a gravimetric reference instrument, the pDR-1200, for $PM_{2.5}$assessment [35]. In the laboratory, the correlation coefficient was 0.97 when incense fumes were used as the particulate matter source. For the indoor environment, the $R^2$was 0.92 when cooking smoke was used, while for the outdoor assessment, the R2 was 0.91 and reached 0.93 when the sensor was calibrated. In addition, the influences of temperature and humidity were corrected. In [39], Sayahi et al. tested both PMS1003 and PMS5003 in the field with a 320-day campaign in which a gravimetric FRM with a 24-hour sampling period and a TEOM (FEM) with a 1-hour sampling period were used as reference systems. The authors sorted the results by different seasons and showed that the results were generally much worse in spring than in the other seasons. The authors obtained the best results in winter, achieving an $R^2$of 0.97 for $PM_{2.5}$with both devices. During the winter, for PM_{10}, the authors also found a correlation coefficient

of 0.91 for PMS1003, and 0.7 for the 5003. When comparing 1-hour sampling data (i.e., TEOM results with LCPMS results for $PM_{2.5}$), the Plantower devices showed comparable performance, reaching 0.88 for the 1003 and 0.89 for the 5003.
Wang et al [17] field tested the recently manufactured Plantower 7003 sensor. The authors evaluated the performance for both $PM_{10}$and $PM_{2.5}$using two different reference devices, a TEOM and an OPC (the GRIMM 1.108). For the TEOM, the correlation coefficient for $PM_{2.5}$was 0.78, while that for $PM_{10}$was 0.73. These values increased significantly, both exceeding 0.96, compared to the OPC, which is based on the same physical principles as the sensor under evaluation.
Compared to the AURN sensors, in [51], the correlation coefficients for two sensors in this family (PMS5003 and PMS7003) for $PM_{2.5}$were 0.76 and 0.73, respectively. Together with the Alphasense N2, Badura et al. [41] field-tested the PMS7003 and evaluated the responses at different sampling times. Correlation results for $PM_{2.5}$measurements yielded an $R^2$of 0.69 for the Alphasense N2 and 0.93 for the PMS7003, calculated against a TEOM 1400a.
In [42], two devices in the Plantower family, the PMS5003 and PMS7003, were field tested using an AURN station as a reference. From the $PM_{2.5}$comparison, the authors obtained correlation coefficients of 0.7 and 0.77. To summarize, this review focused on the Plantower sensors. Despite their cheaper price, these sensors offer good performance and good manufacturing quality.

Novasense SDS011

Another noteworthy competitor is Novasense SDS011, a meter for $PM_{2.5}$and $PM_{10}$with a cost of about $20.
In [19], Cavaliere et al., after calibrating their device in the lab (the device was embedded in an IoT infrastructure along with other gas sensors for comprehensive monitoring of environmental pollutants), compared their results with an ARPAT (the official measurement method in Italy) monitoring unit in a campaign that lasted about 6 months. This device showed excellent performanceproviding R^2values of 0.96 and 0.91 for $PM_{2.5}$and PM_{10}, respectively.

Badura et al. (who tested the Plantower PMS7003 and the ALphasense OPC-N2), also tested a Novasense device [41]. This device provided comparable performance to the Plantower, achieving a correlation coefficient of 0.90 for $PM_{2.5}$.
Hapidin et al. tested their sensor in the laboratory in a special chamber for evaluating low-cost devices for measuring particulate matter [26]. Under these conditions, the Novasense device provided an $R^2$of 0.994 for $PM_{2.5}$.
Despite the small number of scientific papers that have examined the Novasense SDS011, the consistency of the results across tests seems to indicate that this device is one of the best performers in laboratory and field tests.

Other sensors
In addition to the sensors previously discussed, there are several others that have attracted much less interest from the scientific community. The Honeywell HPMA115S0, for example, has only been tested for $PM_{2.5}$. In [26], laboratory tests showed that Honeywell could achieve correlation coefficients as high as 0.99. In [51], field tests provided an $R^2$of 0.77, which was higher than that provided by an Alphasense N2 and only slightly lower than the correlation performance of two Plantower family sensors. In [55], a field test was performed using a Grimm EDM 180, achieving an $R^2$of 0.58 over a 13-day campaign.
Another sensor that falls into this class of devices is the Winsen ZH03A, which was field tested by Badura [41]. The field comparison provided an R^2value of 0.81 but a value close to 1 in the laboratory, which agrees with the results for all other devices. The Sensirion SPS30 is a relatively new sensor whose production started in 2018. Its special features include an ultra-thin package and a HEPA filter to prevent performance degradation due to dust accumulation. The only scientific work that studied its performance showed that this sensor is not suitable for PM_{10}measurements [54]. The last sensor included in this list is the Samyoung DSM501A, evaluated under laboratory conditions in [23]. The reported results showed a very high correlation coefficient of 0.98.

From all these articles, it is possible to outline some useful rules that can

be adopted for the use of these low-cost instruments:

- Relative humidity is a crucial environmental parameter, and keeping the humidity below 85% is important to avoid rapid degradation of accuracy.
- Using high sampling times and averaging data increases the accuracy of PMmeasurements, especially at low PM concentrations ($30\mu g/m^3$for $PM_{2.5}$), where LCPMS suffers the worst accuracy.
- All LCPMS sensors showed the best performance with $PM_{2.5}$.
- The default calibration for an LCPMS is only a recommendation and provides good accuracy only under limited conditions.
- Within the same make and model of LCPMS, quality parameters may vary. Therefore, a lab test is mandatory to verify the quality parameters for each sensor.
- Seasonally specific field calibrations are required for best performance, despite changes in PMtype and humidity interference.

1.7 ENEA PM chamber test

One of the main objectives of the S.A.L.VO. project is to equip the multi-sensory node with a particulate sensor, useful to monitor the environment in which the workers are placed.For this purpose, the research center ENEA in Portici (one of the project partners) has been charged to realize a characterization chamber for particulate sensors.
As seen in the paragraph on characterization in the laboratory, a characterization chamber must be equipped, in addition to reference instruments useful to correlate the performance of the devices you want to test, with a particulate generation system, a ventilation system to homogenize the concentration of PM enclosed in the volume that serves as a test chamber.
After the work of review previously explained, given the objectives of the project and the budget available (about 65000 euros), and after extensive

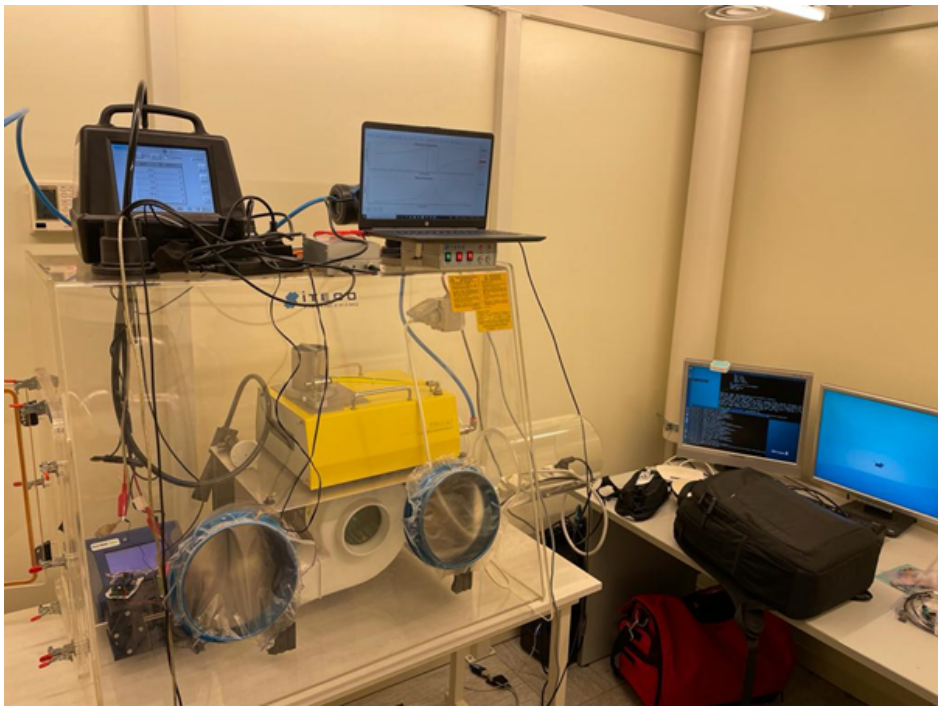

Figure 1.8: Characterization chamber for PM – ENEA

market research and with the help of work in which a chamber is present, the following tools and materials were identified:

- Topas SAG 410 (particle injection)
- TSI DUSTTRAK DRX AEROSOL MONITOR 8533 (OPC reference monitor)
- PARTICLE MEASURING SYSTEMS - IT Lasair III (particle counter)
- Certified powders

Figure 1.8 shows a photo of the characterization chamber with all its instruments on board. As you can see it is enclosed in a glove box of about 500 liters which also houses the above mentioned instruments that we will now describe in detail.

Topas SAG 410

Solid particle aerosols gemerator are used for research, development and quality management in many fields. Powder generators, convey solid material with a dosing belt. This ensures a consistent and well dosed powder powder amount over time. This particular model of powder generator, i.e.the Topas SAG 410 [56], uses the same principle of powder feeding via a special feeding belt. Defined segments ensure constant and reproducible powder feeding even in small quantities. The concentration of the output aerosol particle number can be easily adjusted by setting the feed belt speed in a wide range. Filling of small segments is performed by the scraper. Its design allows a constant powder dosage which is almost independent of the filling level of the powder tank. The reservoir can be refilled during operation without any effect on the aerosol concentration. The dispersion unit consists of a dual flow ejector nozzle and a tube which connects to the compressed air supply housing. The shear forces created in this ejector disperses and deagglomeratesthe powder to form an aerosol.

TSI DUSTTRAK™ DRX aerosol monitor 8533

The TSI DustTrak [57] is portable device and allows, a direct-reading real-time monitoring through a laser light scattering photometer. The photometer operates based on a 90° light scattering configuration illustrated in the section 1.4.1 in which the amount of scattered light is proportional to the volume concentrations, in which the amount of scattered light is proportional to the volume concentrations of an aerosol. The light emitted by the laser diode is scattered by particles passing through the unit as a steady stream. The amount of scattered light determines the mass concentration of the particles based on a calibration factor. The DustTrak has been factory calibrated using ISO 12103-1 A1 (Arizona Road Dust) standard dust. The DustTrak has a mass resolution of $1\mu g/m^3$and a detection range of 0.001-100 mg/m^3 for particle sizes 0.1-10μm. The impaction inputs are used to selectively sample the PM_{10}, $PM_{2.5}$, and PM_1 size ranges at a sampling rate of 1.7 L/min. Therefore, DustTrak instruments were used in this study to measure $PM_{10}$and $PM_{2.5}$, respectively.

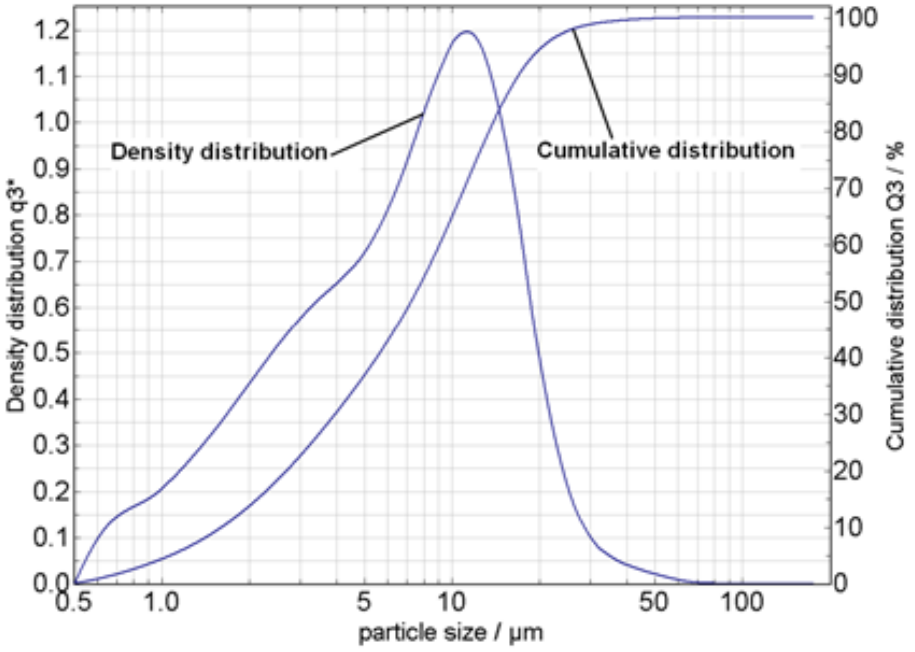

Figure 1.9: Particle distribution by diameter

PARTICLE MEASURING SYSTEMS- IT Lasair III

The Lasair III (Particle measuring systems) is a particle counter used for monitor and certifie the Cleanroom class operations. This instrument is also capable of counting particles of average aerodynamic diameter between $0.3\mu m$ and $25\mu m$ by dividing them into 6 different channel sizes. The device is used to obtain the particle distribution by separating the particles according to their diameter.

Certified powders

For the characterization chamber, certified PM10-like ERM-CZ100 dusts were chosen, i.e. with a distribution of particulate matter around 10 µm in diameter. In Figure 1.9 it is possible to see the particle size distribution according to their average aerodynamic radius and what is their cumulative distribution.

The ideal environment to house the test chamber is a cleanroom, but this

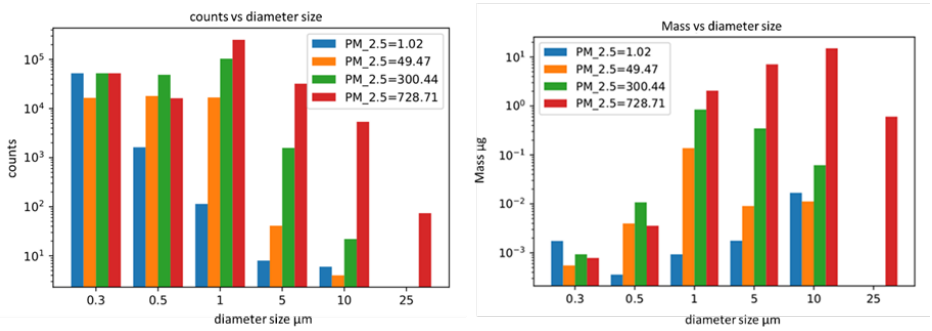

Figure 1.10: on the left the counts of the particles present in the "Odor free Box", detected by the respective dimensional channels; on the right the same data is represented in terms of mass in the air volume

would have posed a contamination problem to the other activities carried out, due to the powders used for the measurements. The possibility of housing the test chamber inside an area called “odor free box”, mainly designed to carry out tests in a quasi real environment on electronic noses,was therefore taken into consideration. The test chamber is located in a room of $2.5 \times 3 \times 2.7m^3$ in an air called Box odor free. This location is equipped with EPA filters which allow the abatement of dust in the surrounding area. Tests were carried out with the aid of LasairIII to understand how resuid particles affected our measurements.

The histograms reported in figure 10 show the different scenarios inside the odor free box, upon the introduction of particles with different concentration (different colors); fig 10.a shows the counts of the particles having a certain diameter, as recorded by the corresponding channel of the LasairIII, as function of the diameter sizes. The second histogram (figure 10.b) reports the same data in terms of mass of particles.

Since the particulate measurement is a mass density measurement with respect to the air volume, the second of the above histograms is the most significant one. From the above data it is evident that, by introducing particulate matter into the test chamber, the masses of the channels corresponding to $PM_{2.5}$and PM_{10}increase at least by an order of magnitude with respect to the background particulate concentration (blue color); this proves that the

background contribution is negligible, validating the choice of the installation of the test chamber in the odorless box.This not only saves space in the clean room, for which the absence of particles is more fundamental than the application of our interest, but also simplifies the use for the operators.

1.7.1 LCPMS in ENEA PM chamber test

In this section will show the test chamber characterizations of some low cost commercial particulate sensors, some of which are also reported in the ref. [58]. The purpose of these measurements is to select the best candidate to be mounted on board the project's target PPE, in the case it is necessary to fall back on a commercial sensor. The tests were carried out by comparing the performance of four LPCMS mounted in the chamber simultaneously and compared with the data recorded by the reference instrument.The tests were performed at three different concentration ranges: 0-40$\mu g/m^3$, 0-150$\mu g/m^3$and 0-700$\mu g/m^3$for $PM_{2.5}$, and 0-250$\mu g/m^3$, 0-600$\mu g/m^3$and 0-5000$\mu g/m^3$for $PM_{10}$from the reference instrument). We will refer to these three ranges as Low Concentration (LC), Medium Concentration (MC), and High Concentration (HC). The comparison between the sensors and the reference instrument is done by following as goodness-of fit parameters those defined by the EPA [59]. namely:

- Accuracy: a measure of the overall agreement of a measurement with a known value. The linear regression coefficient $R^2$is a measure of the precision of an instrument.
- Slope: the incremental change in the response variable due to a unit change in the predictor variable.
- Bias: the systematic or persistent distortion of a measurement process that causes error in one direction.
- Measurement range: the concentration ranges from minimum to maximum values that the instrument is capable of measuring.

The tested devices are as follows:

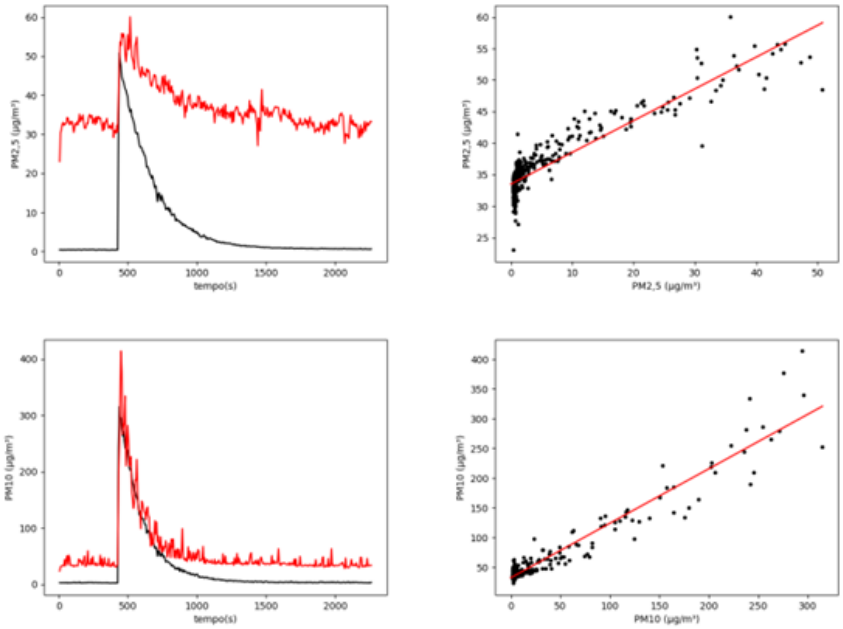

Figure 1.11: in the figure is shown on the right the temporal evolution of PM concentration in the test chamber recorded by Alphasensor (in red) and the reference instrument (in black) in the regime of low concentrations. On the right the scatter plot of the data collected by Alphasense vs the reference device for the two classes of particulate matter

- Alphasense N2
- Alphasense R1
- Novasense SDS011
- Plantower PMS A003

The first measurement we are going to show is related to Alphasense N2 in a regime of low concentrations. in Figure 1.11 the time evolution of the particulate concentration in the test chamber and the comparison between the Alphasense sensor and the reference instrument for the particulate matter $PM_{2.5}$and $PM_{10}$are shown. The results of linear regression by applying the method of least squares, and in particular with the use of a Python library

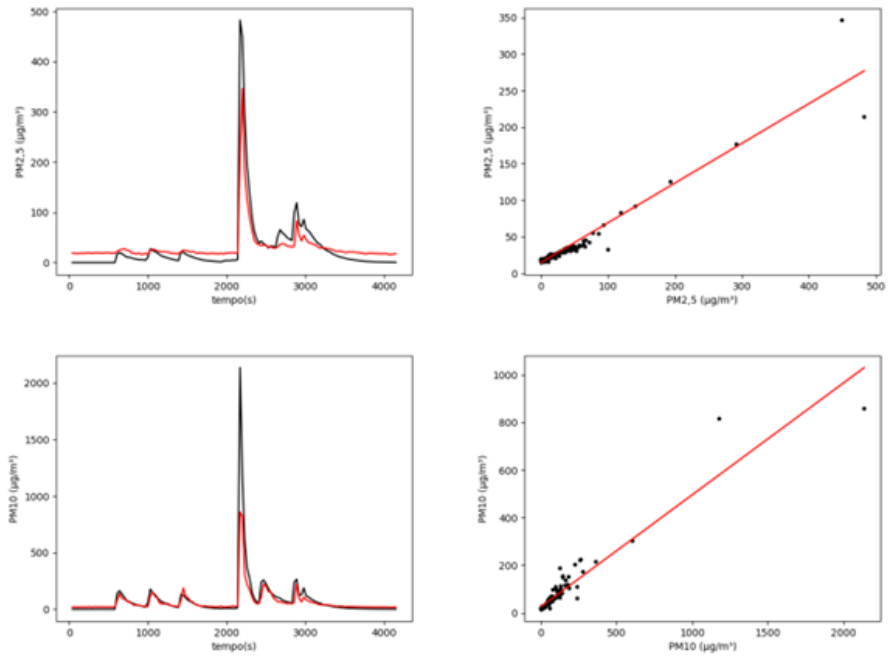

Figure 1.12: in the figure is shown on the right the temporal evolution of PMconcentration in the test chamber recorded by Alphasensor (in red) and the reference instrument (in black) in the regime of low concentrations. On the right the scatter plot of the data collected by Alphasense vs the reference device for the two classes of particulate matter

called Stat model, are the following:

$$y = 0.50x + 33.49 \quad PM_{2.5} \tag{1.5}$$

$$y = 0.92x + 32.52 \quad PM_{10} \tag{1.6}$$

the linear correlation coefficient is 0.83 for $PM_{2.5}$and 0.93 for PM_{10}.
At high concentrations, the sensor under test behaves as shown in figure 1.12. The equations of the best-fit line turn out to be:

$$y = 0.54x + 15.02 \quad PM_{2.5} \tag{1.7}$$

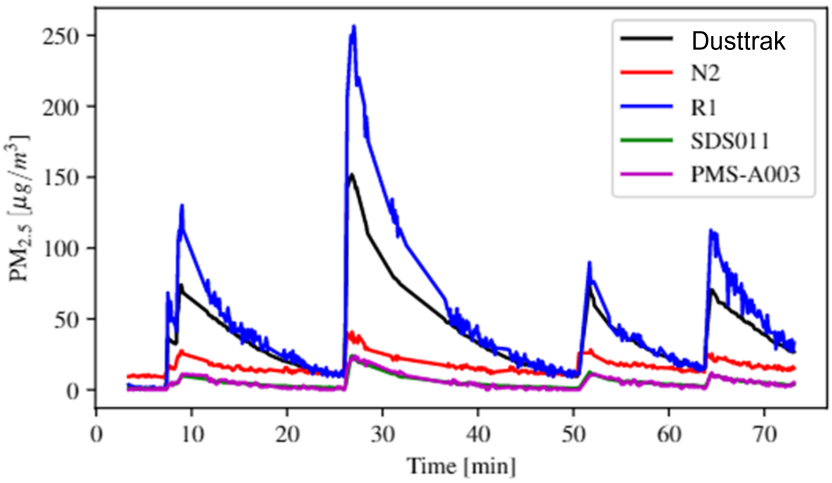

Figure 1.13: Time response to the stimulus of $PM_{2.5}$in the medium concentration range for various particulate sensors

$$y = 0.47x + 25.28 \quad PM_{10} \tag{1.8}$$

In this case the linear correlation coefficients are for the two classes of particulate matter 0.92 and 0.91, respectively.
From another measurement campaign, where 4 of the above mentioned sensors are involved, always in the same concentration range, we report as an example the temporal evolution of the PMconcentration in the medium range in the test chamber (figure 1.13) detected by the sensors.

In table 1.5 we see a summary of what are the results obtained by these sensors. Let's analyze the correlation coefficient of the different PMS at different concentrations:
As can be inferred from the very dispersed plot N2 is not very precise in low range measurements at low concentrations ; at medium concentrations instead it appears to work very well which confirms what said in previous measurements. At high concentrations exceeding 600µg/m3 for $PM_{2.5}$it instead presents a non-linear response , which is not the case for PM_{10}.
R1 works, at low concentrations, performs better than its predecessor N2, goodness that remains in the range of medium concentrations. Like N2 also

		N2		R1		NOVA		PLANT	
		PM2,5	PM10	PM2,5	PM10	PM2,5	PM10	PM2,5	PM10
Data 2 LC	slope	0.178	0.453	1.366	4.130	0.114	0.235	0.085	0.033
	slope error	0.004	0.008	0.012	0.058	0.001	0.005	0.002	0.001
	intercept	14.711	13.369	-0.309	-7.278	0.158	3.022	-0.263	0.103
	intercept error	0.049	0.319	0.134	2.165	0.015	0.189	0.020	0.031
	R^2	0.551	0.674	0.908	0.791	0.872	0.659	0.607	0.489
Data 1 MC1	slope	0.177	0.279	1.538	3.124	0.118	0.260	0.151	0.044
	slope error	0.003	0.009	0.026	0.092	0.003	0.008	0.003	0.002
	intercept	9.948	8.955	-8.211	6.926	0.599	9.846	-0.742	3.034
	intercept error	0.168	1.350	1.308	14.281	0.118	7.993	0.148	0.244
	R^2	0.799	0.592	0.830	0.619	0.774	0.621	0.784	0.520
Data 4 MC2	slope	0.212	0.306	1.881	3.399	0.153	0.391	0.223	0.072
	slope error	0.006	0.014	0.043	0.141	0.003	0.012	0.005	0.003
	intercept	15.701	12.950	-16.078	-20.173	-0.582	9.794	-2.032	5.807
	intercept error	0.362	2.481	2.800	25.444	0.207	2.092	0.355	0.515
	R^2	0.822	0.616	0.856	0.649	0.892	0.792	0.833	0.660
Data 3 HC	slope	0.369	0.321	2.552	3.008	0.302	0.485	0.219	0.079
	slope error	0.003	0.004	0.028	0.041	0.005	0.012	0.003	0.002
	intercept	-2.275	8.158	-108.962	119.437	-16.627	109.515	-3.193	33.051
	intercept error	1.059	4.095	8.667	38.093	1.487	12.075	0.862	1.752
	R^2	0.951	0.901	0.935	0.905	0.905	0.793	0.908	0.744

Table 1.5: Linear regression parameters for various PMSs and the Lasair III for different data sets

it has a non-linear section once exceeded the threshold of $600\mu g/m^3$for the $PM_{2.5}$, something that, also here, is not found in PM_{10}.
As for Novasense, it has a good behavior at low and medium concentrations obtaining better or comparable linear correlation coefficient values than other much more expensive sensors, both for $PM_{2.5}$and PM_{10}.
At medium concentrations it has a good behavior for both classes of particulate matter. The situation is different at high concentrations, where a strong non-linearity is evidenced especially in the PM_{10}class. Finally the Plantower is not able to measure particulate matter at low concentrations, while for the medium range it is able to follow only the $PM_{2.5}$class. Also at other concentrations it shows a problem of non linearity very similar to that found in Novasense.
At low concentrations R1 and Novasense show to be significantly higher than N2 and Plantower for both classes of particulate matter, the values go from 0,5 - 0.6 for N2 and Plantower to 0,8 - 0,9 for R1 and Novasense for $PM_{2.5}$, while the discrepancy is less marked on PM_{10}, in this class of particulate matter N2 manages to have performances comparable with those of Novasense.
At average concentrations we see that Novasense shows the best correlation coefficients for both classes of particulate matter. The other PMS have good correlation coefficients, all above 0.8 for $PM_{2.5}$, while for $PM_{10}R^2$are substantially lower than Novasense, in fact they can not exceed the threshold of 0.7 while Novasense is close to 0.8.
At high concentrations, the sensors are not very linear, this affects the estimate of R^2which for these concentrations we expect close to 1, since at high concentrations the differences in volume sampled between the Dusttrak and PMS matter much less. This is true for $PM_{2.5}$, where the coefficients all abundantly exceed 0.9, while, due to non-linearity, we see the coefficients of Novasense and Plantower fall below 0.8 for PM10.
As far as seen, the best performances are obtained by the Novasense SDS011 and the Alphasense R1. Taking into account the prices of these two sensors, the Novasense about 20$ and the R1 about 300$, it is clear that should a commercial in PPE device be introduced the first choice would be relative to the Novasense.

CHAPTER

TWO

PIEZOELECTRIC MATERIALS FOR PM SENSOR

In this chapter we report the activity carried out, in collaboration with STMicroelectronics, to evaluate the use of MEMS devices based on piezoelectric material, in particular pMUT membranes. After a brief introduction to piezoelectricity, we will then present the structure of the device before showing the characterizations and results obtained.

2.1 Piezoelectricity

Piezoelectricity, discovered in 1880 by Pierre Curie and Paul-Jacques Curie, is the property of some crystalline materials to:

- polarize generating a potential difference when subjected to a mechanical deformation, PIEZOELECTRIC EFFECT to a mechanical deformation, PIEZOELECTRIC EFFECT DIRECT;
- deform elastically when subjected to an electrical voltage, INVERSE PIEZOELECTRIC EFFECT.

For a crystal, to exhibit the piezoelectric effect, it is necessary that its structure does not have a center of symmetry. The structure consists of electric dipoles which, at rest, are arranged in such a way that the faces.

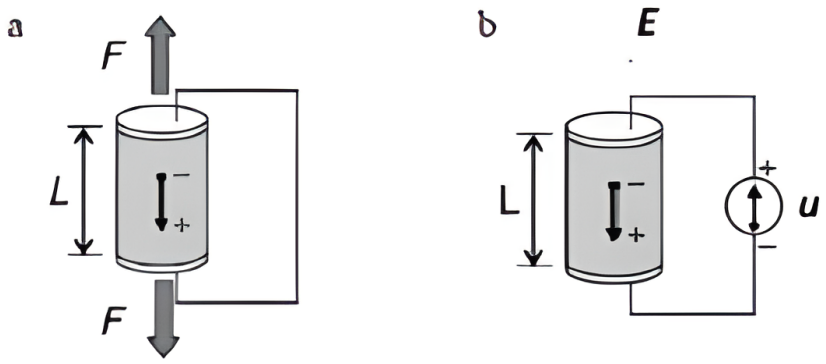

Figure 2.1: piezoelectric effect a) direct b) inverse

Applying a force from outside, the crystal compresses and the structure deforms losing the electric neutrality: one face will be positively charged the other negatively. It will behave like a capacitor to which a potential difference is applied. If the two faces are connected with an external circuit a current called piezoelectric current is generated. Let's consider a cylinder of piezoelectric material with length L and section A interposed between two electrodes in short circuit as in figure 2.1. Piezoelectric effects can be represented by the following linear relationships between the physical parameters of the process: The linear relationship between the stress T_{ik} applied to amaterial piezoelectric material and the resulting charge density D_i is known as the direct piezoelectric direct and is expressed as:

$$D_i = d_{ijk} T_k \tag{2.1}$$

where d_{ijk} is a third-degree tensor of piezoelectric coefficients.
Piezoelectric materials either contract or expand once applied an electric field. The inverse piezoelectric effect describes the deformation S developed in a piezoelectric material due to the applied electric field E. So we can write:

$$S_{ij} = d_{kij} E_k = d_{ijkt} E_k \tag{2.2}$$

The thermodynamic effects from the two direct and inverse d coefficients

$d_{direct} = d_{inverse}$ turn out to be identical.
As can be seen from the formulas, the signs of the piezoelectric charge, D_i, and strain, S_{ij}, depend on the direction of the mechanics and the electric field, respectively. The piezoelectric coefficient d can be positive or negative, and it is in common use to define longitudinal coefficient as the coefficient measured in the same direction as the applied field, transverse coefficient as the one measured in the direction perpendicular to the field.
This coefficient and the other piezoelectric coefficients will be discussed in detail in the following section. once the constitutive equations of piezoelectric materials have been defined. Piezoelectric properties can be intrinsic to some natural materials, such as quartz and materials, such as quartz and tourmaline, or can be generated in artificial crystals. such as Rochelle salt ($KNaC_4H_4O_6 - 4H_2O$) or in piezo-ceramic materials subjected to a process of polarization by means of an external electric field. Two fundamental examples of the latter are: barium titanate ($BaTiO_3$) and lead-zirconate-titanate ($Pb(Zr_x, Ti_{1-x})O_3$), PZT. In the present thesis, reference will be made to the latter.
PZT is a piezoelectric ferroelectric material with high temperature of operation. Microscopically it presents a crystalline lattice similar to that of the mineral Perovskite i.e. face-centered cubic type $A_2 + B_4 + C_3^{2-}$. Above above the critical temperature, Curie temperature (350°), the elementary cell is cubic and symmetric and there is no dipole moment; below the Curie temperature, it is slightly askew and tetragonal, exhibiting a dipole moment other than zero, adjacent dipoles form regions called ferroelectric domains or Weiss domains.
PZT is a solid solution of $pbZrO_3$ (orthorhombic) and $PbTiO_3$ (tetragonal), forming $Pb_2 + (Zr, Ti)_4 + O_3^{2-}$, the structure of which is depicted in Fig.2.2. In the vertices are arranged the large ionic radius metal cations (Pb^{2+}), in the center of the faces the oxygen atoms (O^{2-}) and in the barycenter a confined small ionic radius metal cation (Zr^{4+}, Ti^{4+}). It is a metastable structure, under the action of a mechanical stress or the action of an external electric field, the central atom moves causing an imbalance in the charges giving rise to an electric dipole. The ratio of titanium/zirconium and the possibility

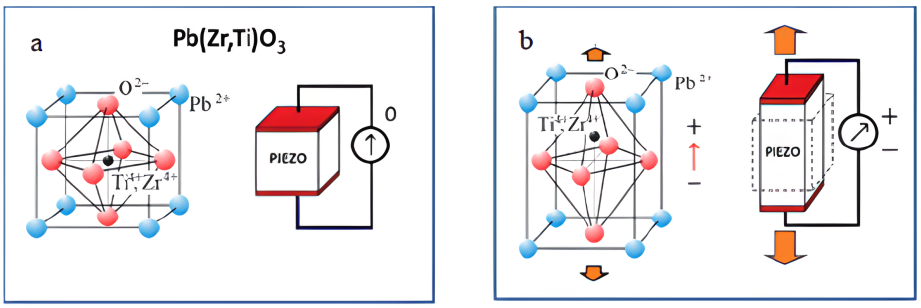

Figure 2.2: PZT structure a) for $T > T_c$;b) $T < T_c$.

of introducing dopants allow great flexibility in terms of composition and therefore functional characteristics.

2.1.1 Constitutive equations

The electromechanical properties of piezoelectric materials are described by constitutive equations. When stressed with a low electric field and at low mechanical stress levels, such materials exhibit linear behavior. In contrast, they exhibit nonlinearity when operated under a high electric field or high mechanical stress, thus showing hysteresis of nonlinearity.
In the case of the linear theory, the quantities involved are the strain S, the mechanical stress T, the electric field E and the electrical induction D. These equations are based on the fact that in the transducer the strain is given by the sum of mechanical stress, induced by the mechanical stress, and drive by the applied electrical voltage. They are valid only under small-signal conditions.
Taking into consideration a triplet of Cartesian axes identified with numbers instead of letters, we identify the x,y,z axes with the triplet 1,2,3 and the three rotation axes θ_x, θ_y, θ_z numbered 4, 5 and 6 as in figure 2.3. Axis 3 is assigned the direction of polarization, obtained during the poling process, and axes 1 and 2 lie in the plane perpendicular to axis 3. The electromechanical equations for a linear piezo are [60]:

$$S_i = s_{ij}^E T_j + d_{mi} E_m \tag{2.3}$$

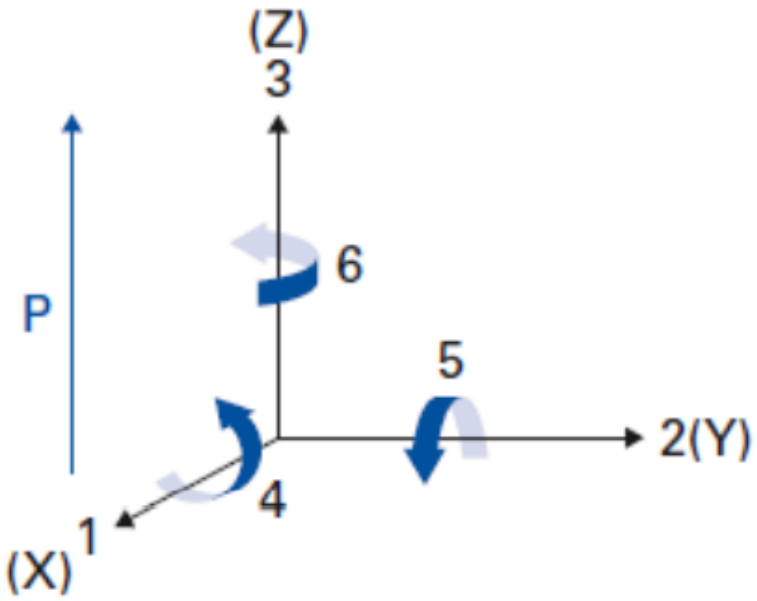

Figure 2.3: Orthogonal coordinate system to describe the properties of a piezoelectric.

$$D_m = d_{mi} T_i + \epsilon_{ik}^T E_k \tag{2.4}$$

where the indices i, j = 1, 2, ..., 6 and m, k = 1, 2, 3 refer to the different directions within the material coordinate system. It is possible to rewrite in the following form:

$$S_i = s_{ij}^D T_j + g_{mi} D_m \tag{2.5}$$

$$E_i = g_{mi} T_i + \beta_{ik}^\sigma D_k \tag{2.6}$$

Where T is Mechanical stress, S Percent strain, E Electric field V/m, ϵ Relative electrical permittivity F/m, d Piezoelectric strain constants, s Conformity coefficients m^2/V, D Electrical induction C/m^2, g Piezoelectric constants m^2/C and β Inverse permittivity m/F.
Equations (2.3) and (2.5) express the inverse piezoelectric effect, describing the situation in which the device is used as an actuator; while equations (2.4) and (2.6) express the direct piezoelectric effect, in which the transducer is

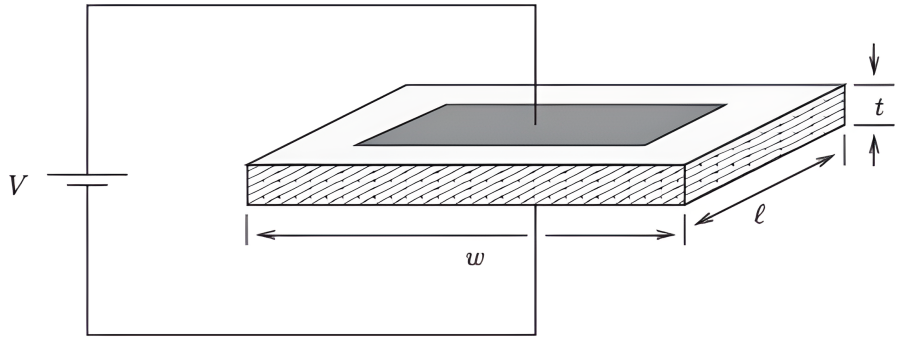

Figure 2.4: Piezoelectric transducer to which a voltage is applied.

used as a sensor.

2.1.2 Piezoelectric coefficients

Let us examine separately the physical meaning of the piezoelectric coefficients : d, g, s.These coefficients, which only describe the material properties under the condition of a small signal, are not independent constants but vary with temperature, pressure, electric field, etc. To these will be added the coefficient k describing the conversion efficiency from mechanical to electrical energy and vice versa.

Piezoelectric deformation coefficient d

The constant d_{ij}, representing the mechanical deformation produced by an applied applied electric field, is defined as the ratio between the deformation developed along the the j axis and the applied electric field along the i axis:

$$d = \frac{\text{developed strain}}{\text{applied electric field}} \tag{2.7}$$

from the figure 2.4 we see that the voltage V is applied to a piezo transducer, of thickness t, polarized in direction 3 , generating the electric field: $E_3 = V/t$
Large d coefficients mean large mechanical displacements.
There is a further interpretation, the d coefficient can be seen as the charge

collected on the electrodes after mechanical stress:

$$d = \frac{\text{short circuit charge density}}{\text{applied mechanical stress}} \tag{2.8}$$

Piezoelectric voltage constant g

It is a measure of the sensitivity of the material: the sensitivity must be sufficiently high so that the generated signal can be detected above the background noise. noise floor. The higher g is, the higher the sensitivity. Also g has another interpretation: it is the strain ratio developed along axis j to the charge (per unit area) deposited on the electrodes perpendicular i-axis.

$$g = \frac{\text{open circuit electric field}}{\text{applied mechanical stress}} \tag{2.9}$$

It is a measure of the sensitivity of the material: the sensitivity must be sufficiently high so that the generated signal can be detected above the background noise. noise floor. The higher g is, the higher the sensitivity. Also g has another interpretation: it is the strain ratio developed along axis j to the charge (per unit area) deposited on the electrodes perpendicular i-axis.

$$g = \frac{\text{unstirred strain}}{\text{applied charge density}} \tag{2.10}$$

Depending on the ways in which the tension can be applied, it is possible to have different g coefficients:

- g_{33} (direct g) is used when the electric field and the mechanical stress are both along the direction of polarization;
- g_{31} (transverse g) is used when the pressure is applied orthogonally to the polarization axis, but the voltage appears on the polarization axis 3;
- g_{15} (shear g) is used when the applied stress is shear and the resulting resulting electric field is perpendicular to the polarization axis 3.

Elastic compliance s

The constant s_{ij} represents the ratio of the strain in the i-direction on the stress in the j direction:

$$s = \frac{\text{developed strain}}{\text{stress}} \tag{2.11}$$

We denote tension and direct stresses with indices 1 and 3 deformations and shear stresses with indices 4 and 6. s_{12} indicates direct strain along axis 1 when the device is stressed along axis 2 and the stresses along 1 and 3 remain unchanged. s_{44} refers to the shear strain around axis 2 due to the shear stress around the axis itself. A superscript E can be found, s_{ij}^{E}, to indicate elastic compliance with the electrodes in short circuit. Or the superscript D, s_{ij}^{D}, if measurements were made with electrodes left in open circuit. A mechanical stress causes an electrical response that can increase the resulting voltage and it is natural to expect E smaller than D; this means that a short-circuited piezo has a smaller Young's modulus of elasticity compared to the open-circuit one.

Electromechanical coupling coefficient k

The coefficient k_{ij}, dimensionless, represents the ability of a piezoelectric material to transform electrical energy into mechanical energy and vice versa. This energy transformation is realized in both piezo materials, i.e., in both sensors and actuators. The index ij indicates that the stress or strain is in the j direction and the electrodes are perpendicular to the i axis.
There are several ways to measure k_{ij}, the most widely used one:

$$k_{ij}^2 = \frac{d_{ij}^2}{S_{ij}^{E} e_{ij}^{\sigma}} = g_{ij} d_{ij} E_p \tag{2.12}$$

i.e., the coupling coefficient can be written in terms of the other piezoelectric constants where E_p is Young's modulus of elasticity of the piezoelectric materia

2.2 pMUT device

Ultrasonic transducer is an important component to realize the conversion between acoustic and electrical energy, used in various fields. Micromachined ultrasonic transducer (MUT) is a new form of ultrasonic transducer produced by microelectronics technology and micromachining processing. It is a thin film MEMS (Micro Electro Mechanical Systems) technology with, often, the presence of a piezoelectric material. MEMS technology uses silicon piezo resistivity or capacitance change to achieve acoustic signal detection. MUT device research, improved design, and micromachining technology make the MUT a promising alternative to the traditional ultrasonic transducer. There are two types of MUTs, the piezoelectric type, pMUT, and the capacitive type, cMUT [61].

2.2.1 MEMS - Micro Electro Mechanical Systems

The term MEMS, Micro Electro Mechanical Systems, refers to devices that integrate mechanical elements on a substrate, for most cases, silicon silicon, with dimensions around the micrometer (typically between 1-10μm) combining the computational capacity of the computational capacity of microelectronics with that of control of micro-sensors and micro-actuators. microsensors and micro-actuators for smart product design.
Such technology, including accelerometers, gyroscopes, piezoelectric devices microphones, etc., represents a revolution in the telecommunications industry, automotive, consumer, IoT, industrial and medical sectors. Its significant advantages are compact size, low power consumption (low leakage and low power consumption), low cost, and higher reliability (it has an effective response time much faster than macro-scale solutions).
The fact that microsensors, microactuators, microelectronics, and other technologies can be integrated into a single microchip represents one of the most important technological innovations.
Fabrication techniques can be classified into two methods:

- Bulk micromachining

- Surface micromachining

Surface micromachining is done by depositing, shaping and etching a sequence of thin films, making the structure free to move above the substrate surface; in bulk micromachining, features are shaped (deposited and removed) to form functional components of the resulting device by dependent orientation (anisotropic) or independent orientation (isotropic).

2.2.2 Thin Films

Thin Films are defined as layers of materials with thicknesses varying between fractions of nanometers and several microns, obtained through a process of deposition on the surface of a given material, called substrate. Film and substrate are made of different materials and therefore characterized by different refractive indexes. The material that goes to form the deposit is called source material and can be of nature (metallic, alloy, magnetic, insulating or semiconducting). Thin films are often used to modify or improve the characteristics and performance of the substrate material on which they are made. The process of application on a surface of a thin film is called deposition. There are several techniques for film deposition, many of which are based on processes that occur at pressure much lower than atmospheric pressure.
They differ mainly on the basis of the physical state in which the material is found. source material and mainly three categories can be distinguished:

- Film deposition from solid phase (e.g., precipitation methods);
- Deposition of films from liquid phase (e.g., plating);
- Gas (or vapor) phase film deposition;

The latter technique is divided, in turn, into two broad categories depending on whether the process is essentially chemical (CVD) or physical (PVD). In CVD a fluid undergoes a chemical change when it comes into contact with the surface of a solid, the fluid surrounds the solid, and deposition occurs over the entire surface, covering it. over the entire surface, covering it uniformly.

PVD uses mechanics and thermodynamics to produce thin films of solids. In this step, the material to be deposited is placed in a region of the vacuum chamber (source), due to the high energy acquired the particles escape from the escape from the surface of the source and travel to the substrate, which cools the particles that bombard it. cools the particles that bombard it, allowing the formation of a solid layer. solid layer. Since the particle trajectory is generally a straight line, the deposited film tends to be directional.
Almost all films, regardless of the deposition process, have an internal stress layer. It may be:

- Compressional, the film tends to expand parallel to the surface;
- Tensile, the film contracts and if the stress exceeds the elastic limit, it breaks in some areas in some areas;

The refractory metals are those that generally have the highest stress, while the metals soft metals (Copper, Aluminum, Gold, Silver) generally have small stress. The substrate temperature allows to control the stress, but a big role is played by the type of substrate. the type of substrate used. The stress measurement is done accurately with X-ray diffraction but also by depositing films on very thin substrates and measuring the deformation.

2.2.3 PiezoMEMS

PiezoMEMS are microelectromechanical systems in which piezoelectricity is used as an actuation and sensing mechanism. The actuation of MEMS could also be done electrostatically or magnetically, but piezoelectric actuation piezoelectricity, in addition to having high sensitivity, allows it to work with low voltages and to operate at low power and therefore involves a lower consumption of energy (it is a few millivolts). They exploit an electrical potential that appears as mechanical stress. The most promising piezoelectric material is PZT, lead zirconate titanate, because of its high piezoelectric coefficient d_{ij}, its tunable dielectric constant, eij, and the coefficient of electromechanical coupling, k_{ij}.
Such devices can be found in numerous applications, and beyond transducers

ultrasonic, pMUTs (analyzed in this thesis), switches, microphones, micro-mirrors, various probes and sensors, energy harvesters, etc.
This versatility of theirs led to the creation of piezoelectric thin films that have contributed to the realization of highly integrated piezoMEMS devices. There are three main approaches for the realization of such devices:

- Additive approach, in which piezoelectric thin films are deposited onto silicon substrates with insulating and conducting material substrates followed then by surface micromachining or bulk silicon;
- Subtractive approach, in which piezoelectric (monocrystalline or polycrystalline) and piezoceramics undergo bulk micromachining;
- Integrative approach, the structures being worked on are integrated on silicon or piezoelectric with bonding technologies on bulk piezoelectric or silicon substrates; [62].

Despite advances in deposition methods, processing, patterning and integration very few piezoelectric devices are still commercially available, it remains an open challenge from a fabrication point of view, e.g. for the deposition of piezoelectric films chemical solution methods are preferred being cheaper, however such methods are based on the use of multilayer materials requiring numerous development efforts for the devices themselves. In addition, researchers continue to seek ways to reduce and control material and sensor drift and aging characteristics of thin film piezoelectric materials. Significant challenges verify optimizations of residual stress in individual layers and the development of deposition techniques that result in thin films with properties that approach those of bulk materials [62].

2.2.4 MUT

MUTs are one of the applications in which MEMS technology is expected to offer significant advantages over the ceramic mass transducers used to date. ceramic mass transducers used to date. They utilize the "flex-tensional" vibration of an array of micro-membranes [63]. They are divided into two

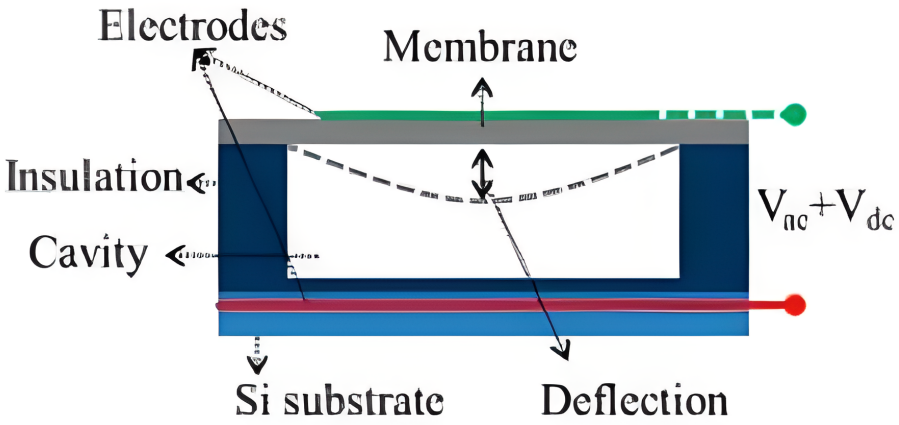

Figure 2.5: cMUT schematic image

categories: cMUT and pMUT, capacitive and piezoelectric ultrasonic transducers, respectively, depending on the actuation principle, electrostatic or piezoelectric. The performance of these miniaturized ultrasonic transducers is showing a strong possibility to replace conventional ultrasonic transducers. Both, like classical transducers classical, have two principles of operation: reception and transmission.

cMUT

Capacitive microscopic ultrasonic transducers (cMUTs) are made of thin silicon nitride membranes, which are essentially parallel plate capacitors with a space between them. Specifically, it can be described as a thin moving plate suspended over a space. The metal on top of the thin plate, or the thin plate itself if it is conductive, forms the top electrode of the capacitor and the lower conductive substrate acts as the bottom electrode. There is a representative image of the device in figure 2.5: When a DC voltage is applied between the two electrodes, the movable plate is attracted towards the substrate by the electrostatic force, which is balanced by a mechanical mechanical restoration due to the stiffness of the plate [64]. In transmission mode, the membrane is driven by an alternating current at its resonant frequency, and large displacements and, consequently, significant sound generation. In contrast, in the receive mode if the membrane is properly polarized and subjected to ul-

trasonic waves at a resonant frequency on the electrodes, significant sensing currents will be generated. significant. The generated electrostatic force, F_{cmut}, is calculated as:

$$F_{cMUT} = \frac{C_0(V_{dc} + V_{ac})^2}{2g_0} \tag{2.13}$$

where the voltages V_{dc} and V_{ac} are the bias and drive signal, respectively, g_0 the thickness, or gap thickness, and C_0 is the capacitance; thus the amplitude of this current is a function of the frequency of the incident wave, the bias voltage, and the capacitance of the device.
The frequency of the vibrating membrane is twice the frequency of the applied AC voltage because it is the unipolar electrostatic force. Therefore, a required a DC bias voltage, which is greater than the amplitude of the AC voltage, for proper operation of the cMUT, because it is useful for detecting the vibration harmonic of the membranes from an incident acoustic wave. In this way cMUTs detect the acoustic wave reflected from an object.
To date, the first integrated devices with cMUT devices are already on the market and show advantages over conventional piezoelectric transducers. However, there are still practical limitations both on the functional side and in manufacturing. From a From a functional point of view it is difficult to guarantee a safety margin to avoid a collapse on all array elements due to bias voltages. In addition, it is difficult to obtain the theoretical coupling coefficient precisely because to to obtain it the bias voltage must be close to the collapse voltage of the device. of the device.
Another limitation is the need of different designs to transmit and receive signals: in order to increase the sensitivity of a receiving element, the space in the to increase the sensitivity of a receiving element, the membrane gap should be small, while the membrane gap for a transmitting element should be large enough to allow for a large bending large bending that generates a strong sound wave. This brings complexity in its fabrication on the same wafer.

pMUT

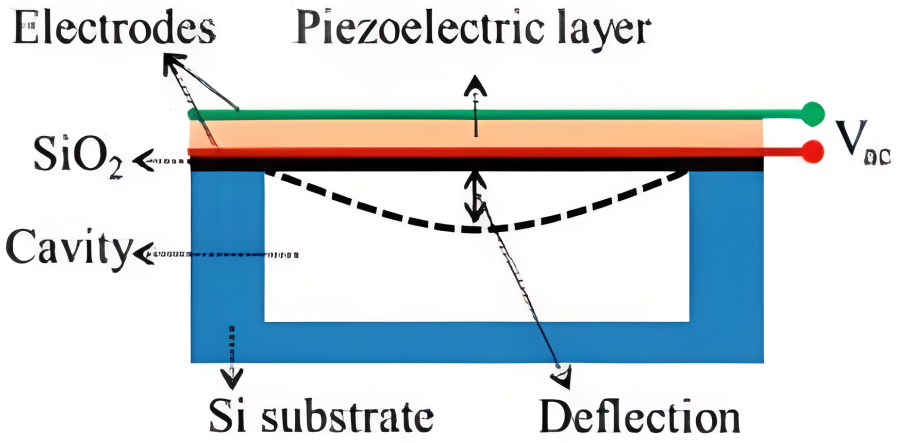

Figure 2.6: pMUT schematic image

pMUTs are thin-film piezoelectric structures that are finding a wide variety of applications in emerging technologies. They consist of the integration of thin films of PZT (lead zirconate titanate) material on silicon substrates. The single device consists of a piezoelectric thin film placed between two electrodes, respectively top electrode and bottom electrode. The whole assembly constitutes the vibrating membrane, fig. 2.6 The lateral dimensions of the membrane are on the order of tens of microns to allow vibrations in the MHz range. The devices used in the present work consist of plates layered with a piezoelectric layer, PZT, used to emit and receive ultrasonic waves. Specifically, circular plate models consisting of silicon, Si, and PZT layers were analyzed. The PZT, i.e., the active piezoelectric layer, is deposited on an elastic silicon membrane which is the passive layer and is sandwiched between two metal layers that act as electrodes, respectively called bottom electrode and top electrode.A structure so made is also referred to as unimorphic structure and its schematization can be seen in figure 2.7 The device, once an input voltage is supplied, starts to vibrate and emits an acoustic signal. Any material, within its elastic regime elastic regime, is subject to a linear stress-tension relationship when compressed or expanded. This is characterized by the material properties, Young's modulus E_i and its geometry. The contraction or expansion perpendicular to the force applied is

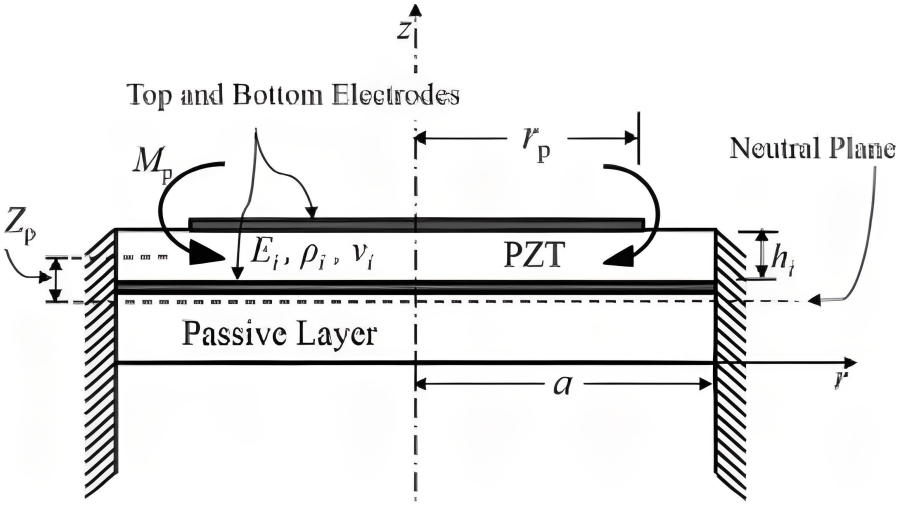

Figure 2.7: pMUT scheme

characterized by the Poisson's ratio ν_i.

When arching the modulus of Young is not sufficient to fully characterize the problem. We know that the membrane of the pMUT vibrates with a specific frequency and it is the mass of the membrane itself that affects the dynamic behavior depending on its density ρ_i.

The resistance of the medium influences in the vibration as a load and is characterized by its acoustic impedance, which depends on the frequency. The piezoelectric material relates the stiffness of the membrane to the electrical domain and it is because of this multi-domain dependence that the membrane cannot be characterized in isolation, but is described through an equivalent circuit approach.

The vibrometric characterization allows to obtain the vibrational spectrum and to analyze the device in the time domain. analyze the device also in the time domain; that is, it provides a dynamic analysis of the object. analysis of the object. Through this aspect it is possible to see all the vibration vibration modes of each membrane and obtain its mechanical information. mechanical.

The electrical characterization allows us to study the device through equivalent circuits and to derive from them the equivalent circuits and derive from

them the characteristics of the elements of the array.

2.2.5 Vibrational Mode

Every vibrating system, be it mechanical, electrical or acoustic, possesses particular modes of oscillation in which all of its component parts vibrate with harmonic motion and with the same frequency. These are the normal modes of the system. To each normal mode corresponds to a particular frequency (called the frequency of the system). system), not vice versa: the same frequency can correspond to different modes in which different modes in which the oscillators have different phase relationships between them.
Each mode is uniquely characterized by its own frequency (or eigenvalue of the mode) and the initial conditions of the system. (or eigenvalue of the mode) and the initial conditions of motion for all oscillators (eigenvector of the mode). mode). Normally a physical system does not oscillate according to only one of its normal modes, but according to a combination of them (eigenmode), but according to a combination of them (superposition).
The superposition of normal modes gives as a result a valid mode of vibration but no longer normal. The Fourier theorem tells us that any mode of vibration (normal or not) can be considered the sum of an appropriate number of normal modes. normal modes.
Let us consider a circular membrane perfectly elastic and fixed along the whole edge. Its normal modes are characterized by two integers where:

- n characterizes the tangential, or angular, oscillation (i.e., along the concentric circles concentric circles);
- m characterizes the radial oscillation (i.e. along the direction that goes from the center to the edge).

So fixed the radius of the membrane the frequency of each mode is determined by these two numbers determined by these two numbers: the first one indicates the number of nodal diameters, the second the number of nodal circles (including the edge always present). A diameter or a circle is nodal when it is always at rest during oscillation.

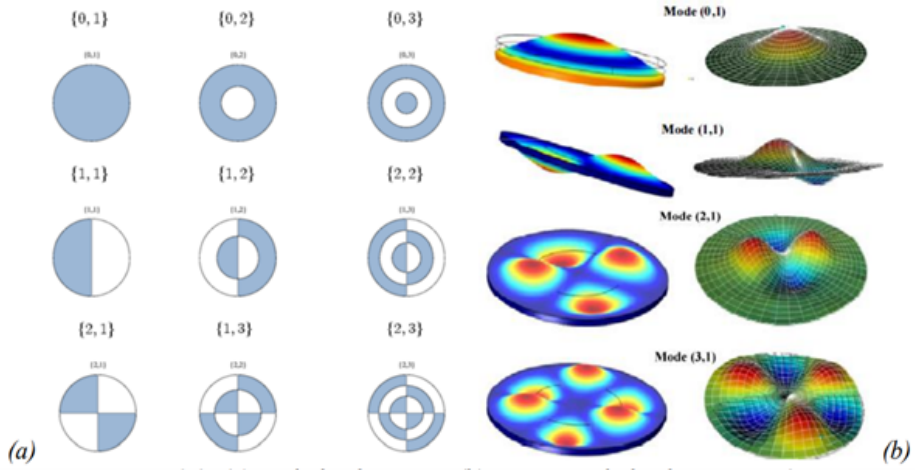

Figure 2.8: (a) vibration modes; (b) example vibration modes in 3D.

For example, the mode 0,1 means that there are no nodal diameters but there is a nodal circle. In figure 24 (a) are represented some examples of vibration modes; the areas colored in blue indicate the areas of the membrane that vibrate in phase opposition to the areas in white; the lines in black are nodal lines and are areas of the membrane always at rest for that particular mode. In figure 24 (b) instead, there are four 3D vibration modes of the membranes covered by this work. The modes of a membrane are transverse standing waves that vibrate each of its points of pure harmonic motion. A transverse wave is defined as a vibration perpendicular to the direction of propagation. A membrane propagates along the plane in which it lies, but the vibration occurs perpendicular to that plane. The study of normal modes allows us to decompose an oscillatory motion, even complex, in simple harmonic components, revealing the internal dynamics of the system.
The motion of the membrane is very similar to that of a vibrating string, but while the latter is a one dimensional body, the membrane has two dimensions, therefore its vibration modes are expected to be richer than those of a string. The normal mode is a vibration in which every point of the membrane moves with pure harmonic motion. Harmonics, the further they are from the fundamental, the less they contribute to the timbre because they are less ample, but, above all, less audible.

The oscillation of a membrane subjected to stress is described mathematically by an equation mathematically by a differential equation of the second order whose solution is obtained using Bessel functions. This equation, describing small displacements, is a function of position and time: $z = z(x, y, t)$).

2.2.6 Electrical Behavior: Equivalent Circuits

Let us now look at the circuit representation of such a device. As we have said several times the electroacoustic transducer is a vibrating device that as an emitter is set in motion by the applied electrical voltage and radiates sound; as receiver the wave arrives on the device generating an electric signal. So, it is in part acoustic (on the moving surface that is in contact with the acoustic medium), in part mechanical (as a acoustic medium), partly mechanical (as a moving body controlled by forces) and partly electrical (as a current controlled by voltage). There are circuits equivalent circuits represented the transducer that of it make possible a simulation electrical facilitating the analysis and design.
In order to arrive to describe the equivalent circuits we analyze the physical situation that presents us; the simplest comparison is that of a harmonic oscillator in the situation reported in figure situation shown in the figure or a spring and a load R tied to a mass M, figure 25 where F is proportional to the voltage or current, the spring has stiffness k =1/C with C conformity and R mechanical resistance. We then denote by x the displacement of the mass with a velocity u=dx/dt.In a typical piezoelectric transducer, the force $F = N_V V$ where V is the voltage and N_V is the transduction coefficient, the spring is the piezoelectric material, and the mass is the radiating piston. The equation of motion for such a model is written in terms of the following. velocity:

$$F = M\frac{du}{dt} + Ru + \frac{1}{C}\int udt \tag{2.14}$$

Since the dynamic system can be modeled using differential equations, there are several ways to model, analyze, and estimate the behavior of such devices. The most widely used models are the Mason model, which is an electrical equivalent of the equations of motion including the piezoelectric, and the

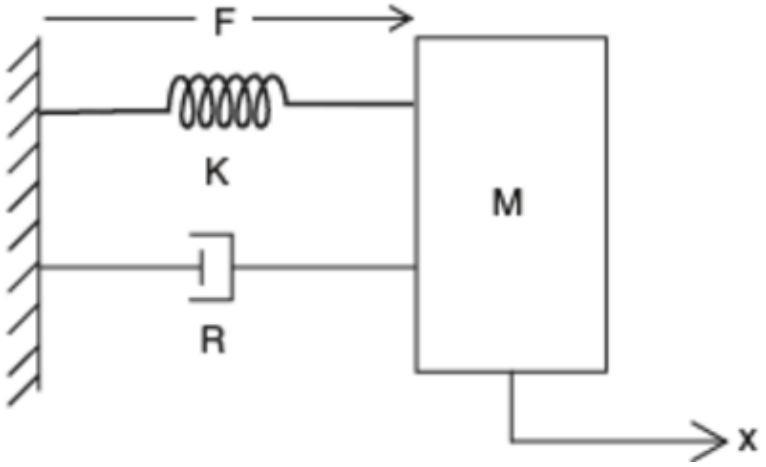

Figure 2.9: Mechanical Oscillator

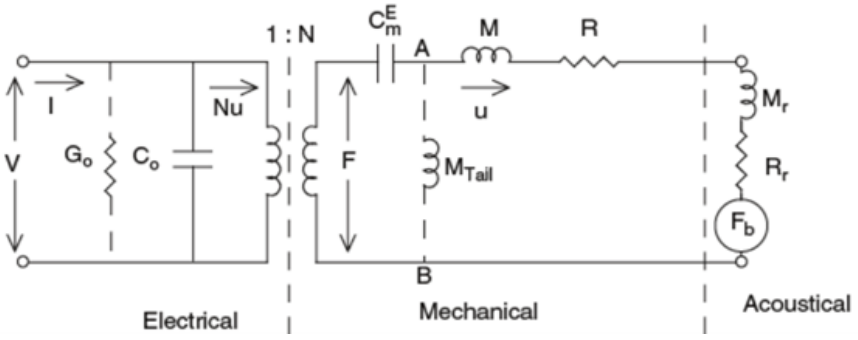

Figure 2.10: Mason model

Butterworth-van Dyke equivalent circuit [65].

2.2.7 Mason model

Mason's model relates all three characteristics of the transducer, i.e., the acoustic, mechanical, and electrical parts figure 2.10 The section to the left of the transformer is the electrical part that represents the locked electrical admittance under conditions where $u = 0$. The section on the right side of the transformer is called the motion part of the circuit, and an impedance or motion admittance is associated with it. We denote by V the voltage applied to the piezo that is used to charge the electrical capacitance C_0 and

generate a piezoelectric force on the system. The electromechanical coupling N describes precisely the piezoelectric effect, i.e. the conversion of electrical energy into mechanical energy. The mass of the system is represented by the inductance and describes the inertia of the system. A high value will bring the resonant frequency downward. The capacitance C_m^E is equivalent to the inverse of the system stiffness k and a high value of it high (so a low value of C_m^E) increases the resonance frequency of the system. Finally, the resistance R is equivalent to the damping of the system c which depends mainly on the materials used. High damping will result in a slower slower but stable response.
The equation of motion can be written:

$$F = NV = (M + M_r)\frac{du}{dt} + (R + R_r)u + \frac{1}{C^E}\int udt \tag{2.15}$$

The solution for speed can be written as : u=NV/Z. where Z is the mechanical impedance.

2.2.8 The Butterworth-van Dyke model

The Butterworth-van Dyke (BVD) model allows to study the electrical behavior of the transducer around its main resonant frequency. of the transducer around its principal resonant frequency. In this model, the moving elements of Mason's model are converted into electrical elements. electrical elements. It is schematized by the circuit in Figure 2.11 It consists of an RLC series branch in parallel with a capacitance C_0 representing the capacitance of the piezoelectric material. To this is often added a resistor R_0 parallel to C_0 needed to model any dielectric and mechanical losses. The impedance trend as a function of frequency is schematized in figure 2.12: at the ends the RLC branch is cancelled and only the R_0/C_0 circuit is seen. In the middle part we have resonance, in which there is the series RLC branch, and antiresonance, parallel RLC.
This electrical model represents the purely electrical part of the transducer through the capacitance C_0, and models the mechanical part of the Meson

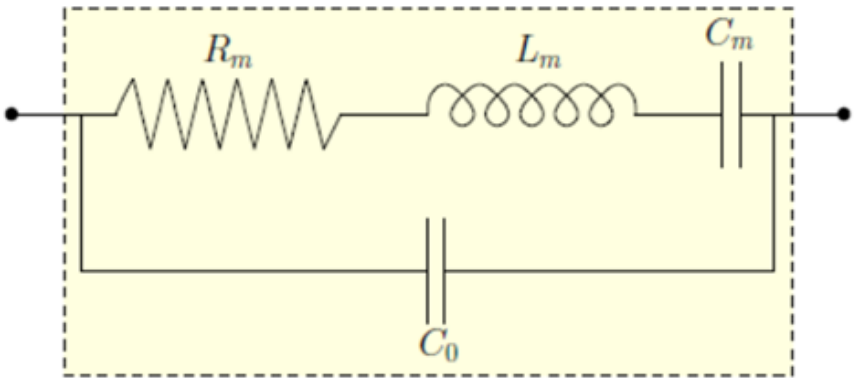

Figure 2.11: Butterworth-van Dyke model

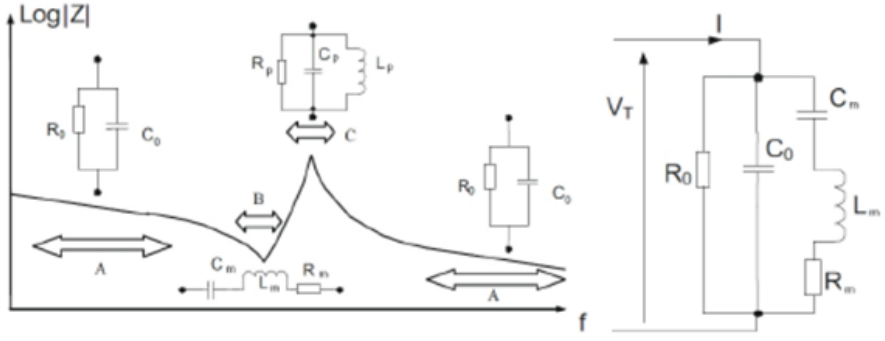

Figure 2.12: Frequency-dependent impedance trend

circuit, through an equivalent circuit called "motional circuit" that allows to study the transducer impedance the impedance of the transducer through the physical parameters of it:

$$C_m = N^2 \tag{2.16}$$

$$L_m = \frac{M + M_r}{N^2} \tag{2.17}$$

$$R_m = \frac{R + R_r}{N^2} \tag{2.18}$$

Such a model is especially useful if one is interested in studying the behavior of transducer impedance as frequency varies.
Fundamental to be able to determine the parameters of the circuit are the resonance frequency (also known as frequency in series f_s) and antiresonance frequency (frequency in parallel f_p) for which the formulas are valid:

$$f_s = \frac{\omega_s}{2\pi} = \frac{1}{2\pi\sqrt{L_m C_m}} \tag{2.19}$$

$$f_p = \frac{\omega_p}{2\pi} = \frac{1}{2\pi\sqrt{L_m \dfrac{C_0 C_m}{C_0 + C_m}}} \tag{2.20}$$

Near the series frequency the device impedance reaches a minimum value that coincides with the value of resistor R_m, while in the vicinity of the parallel frequency the impedance reaches a maximum value, in a neighborhood of the value of resistor R_0. They will be fundamental for data analysis.

2.3 pMUT as PM sensor

In this section we will see the characterizations that led to the use of this type of device as a particle detector first and then to the realization of a prototype of a particle sensor based on the same.
To perform this analysis, in addition to the particle chamber presented in the

previous chapter, the Polytec SA-500 Micro System Analyzer, Figure 2.13, with its corresponding software. It is a laser Doppler vibrometer and is useful to determine the vibration velocity and displacement of the membrane. It works by detecting the shift in the frequency of light scattered on the moving surface. The object scatters or reflects the light from the laser beam and the change in of frequency by Doppler effect is used to measure the component of the velocity located along the axis of the laser beam. The device is placed on the metal plate placed under the head of the instrument; inside it there is a camera which allows the visualization of the device both on pc and on the screen with which it is equipped; moreover it is incorporated of a laser with which the measurement is carried out, figure 2.14; externally there are four Externally there are four lenses where, excluding one for topographic measurements, the others allow different allow for different magnifications. The instrument is located on top of an anti-vibration table for the purpose of to attenuate ground vibrations and not interfere with the measurements. the measurements. The structure under exam is a clamped multilayered circular diaphragm with a radius of $440\mu m$. It consists of a $2\mu m$ thick piezoelectric layer (PZT) with radius of $308\mu m$ sandwiched between two 100nm thick metal electrodes all deposited onto a $4.25\mu m$ thick passive thin film of silicon layer (passivation layers are not reported). The transduction principle of the resonator is the mass loading effect, i.e. an addition of a mass to the membrane results in a shift in its resonant frequency.

The resonance frequencies of a membrane are dependent on the characteristic properties of the materials involved in the structure-stack [65] and are described by

$$f_{mn} = \frac{1}{2A}\alpha_{mn}\beta_{mn}\sqrt{\frac{D}{\rho}} \tag{2.21}$$

where A is the membrane area, D is the equivalent flexural rigidity, $\rho = \sum_{i=0}^{K} \rho_i h_i$ is the mass per unit area, ρ_i,h_i are mass density and thickness of the i-th layer in the stack, K is the number of layers and the product $\alpha_{mn}\beta_{mn}$ represents the non-dimensional frequency parameter for the circular plate.

When a small extra mass Δm is added to the surface, the resonance spectrum will be affected by the increased mass of resonance structure. The extra mass

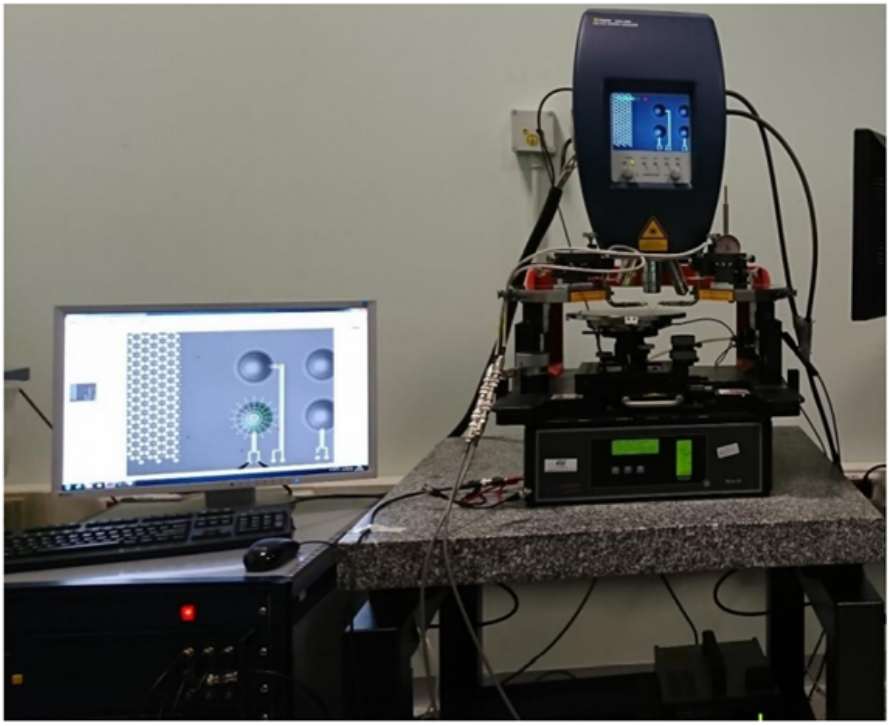

Figure 2.13: MSA-500 Polytec

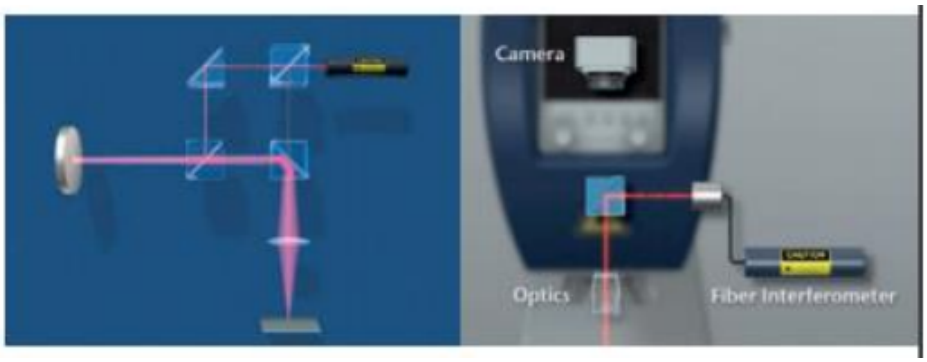

Figure 2.14: Polytec's internal laser scheme

is approximated by an additional homogeneous nonstructural top-layer onto the structure stack with the density $\rho' \approx \ \rho + \frac{\Delta \mathrm{m}}{A}$. The resonance frequencies will decrease and if Δm is much smaller than the effective mass $m_{eff} = A\rho$ of the diaphragm itself then the frequency-shift Δf_{mn} can be considered as proportional to Δm. This assumption will lead to $\Delta f_{mn} = -\frac{\Delta m}{2m_{eff}}$ where f_{mn} is the frequency without the additional mass. The mass sensitivity can be estimated by the relation

$$S_{mn} \approx -\frac{\Delta f_{mn}}{\Delta m}. \tag{2.22}$$

For a membrane with a given normalized sensitivity we can calculate *Deltam* by measuring the frequency-shift.
On the other hand, we can evaluate experimentally the mass sensitivity by loading small calibrated extra masses onto the membrane surface and measuring the frequency shift. For the sake of simplicity, we will define the normalized sensitivity $S = \frac{S_{mn}}{f_{mn}} = \frac{1}{2m_{eff}}$ and we will estimate it by analyzing the frequencies shift of the first three vibrational modes as function of certified microbeads loading.

2.3.1 Characterization

The mass sensitivity of the membrane is evaluated by using certified monodispersed Silica and non-porous microspheres (aqueous suspension) with diameter of $5\mu m$ (std dev $< 0.35\mu m$) and density range 1.800-2.000g/cm^3. The experimental procedure provides the acquisition of the initial frequency spectrum of the membrane free from particles. Subsequently the silica microbeads are loaded at membrane surface (Fig 2.15) by dispensing micro-drops of the aqueous suspension at 27°C of stage temperature. The vibrational spectrum is continuously monitored in the meantime camera images are acquired showing the membrane surface. Once the drop lies onto the surface it starts to evaporate and finally the vibrational spectrum will depend just on what remains on the surface.
Before loading the particles, trials of dispensed micro-drops free from silica

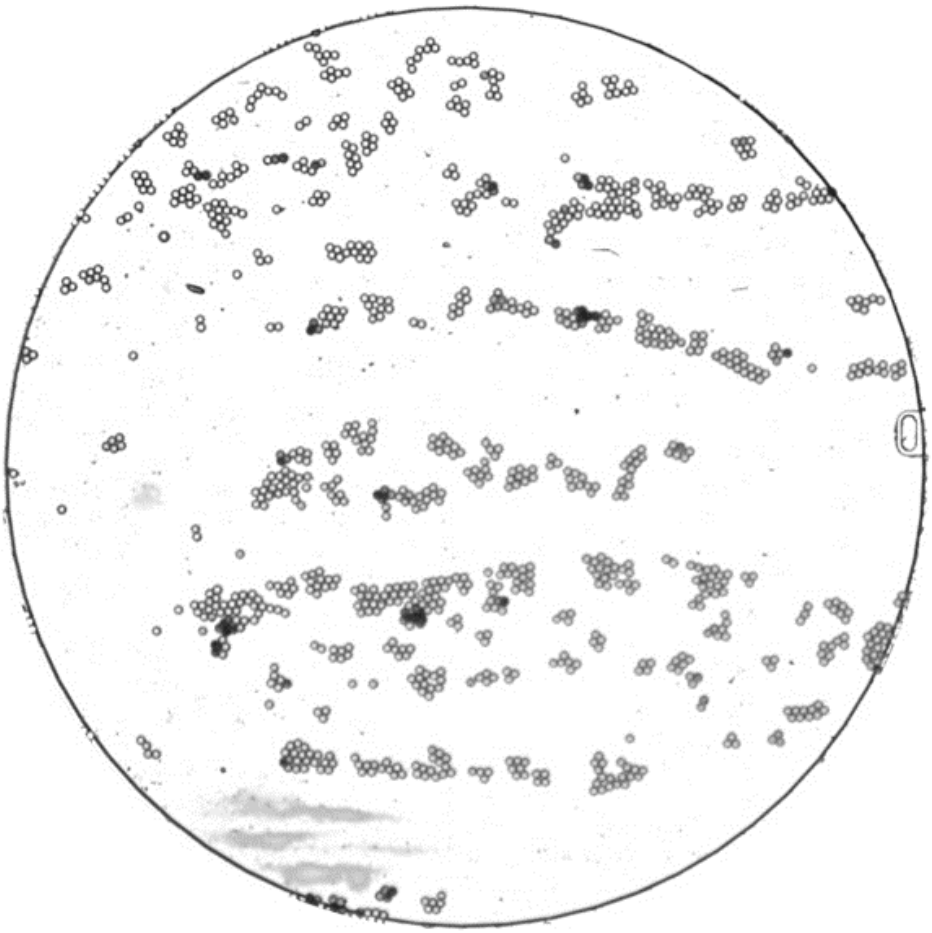

Figure 2.15: image of the membrane with N loaded numbers of beads

were made and the time (t=10' doubled the minimum) to wait till the drop is completely evaporated was estimated. The membrane is then free from solution and the vibrational spectrum turns back to its initial values. The experimental analysis continues by positioning the microbeads. A micro-drop containing silica beads is dispensed onto the membrane and after 10' we acquire the vibrational spectrum plus camera images.
The microbeads were then partially removed, and a new spectrum was recorded together with the corresponding microscope images. The number N of loaded micro-beads was derived subsequently by processing the acquired images plus a visual inspection. The mechanical removal process was iteratively conducted till the membrane surface reached the state free from beads and the

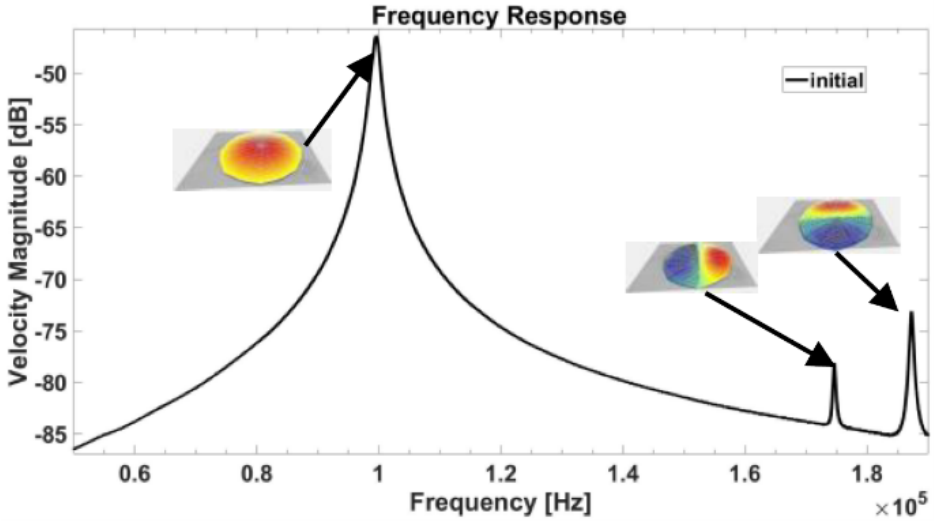

Figure 2.16: Initial frequency spectrum (dB-Reference: 0 dB = 1 m/s) measured in air showing first three resonance modes and their mode shape

corresponding spectrum matched the first initial acquired. The mass of N beads is derived by $\Delta m = (\pi/6)N\rho_s d^3$ where use was made of the tabulated density of $\rho_s = \frac{2.000gr}{cm^3}$ and diameter $d = 5\mu m$.
The frequency response of the membrane was measured in air via a laser doppler vibrometer (LDV, MSA-500 Micro System Analyzer, Polytec). A periodic chirp signal with the amplitude of 0.1V actuates the DUT (device under test) whose vibrational spectrum is consequently acquired with a resolution of 10Hz. The DUT shows the first three resonance (Figure 2.16) frequencies: $f_{1st} = 99586Hz$; $f_{2nd} = 174617Hz$;$f_{3rd} = 187273Hz$. The values of resonance frequencies are affected by the materials pre-stresses and some source of inhomogeneity in the structure. Further, the separation of the two degenerate modes (f_{2nd} and f_{3rd}) can be ascribed to the asymmetry breaking coming from structure as result of some source of uncertainty from the process to make this particular prototype.

In Figure 2.17 we report the initial spectrum and a shifted one due to the beads deposited onto the surface. The spectra report the velocity acquired highlighting that the velocity mismatch is negligible in the linearity regime of working principle. The complete set of acquired data are graphed in Figure

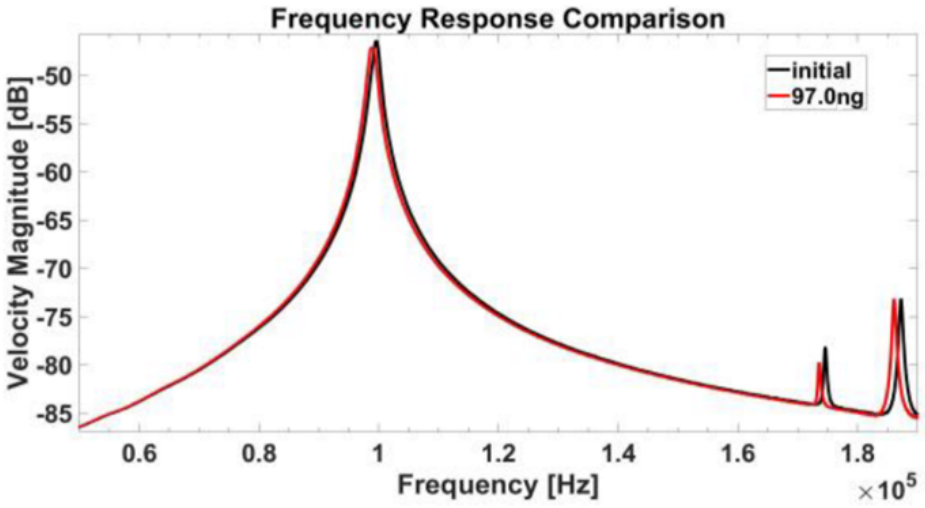

Figure 2.17: Initial frequency spectrum (dB-Reference: 0 dB = 1 m/s) measured in air showing first three resonance modes and their mode shape

Table 2.1: normalized sensitivity from data fit for the first three modes

mode	S (10^-5 ng^-1)
1	5.5±0.3
2	6.2±0.2
3	6.0±0.2

2.18 where the frequency shift data for the first three resonance modes at different loading steps is reported. The fitted parameters are reported in the Table 2.1 According to the fitted data we can also derive the sensitivities for the three vibrational modes. In particular focusing on the 1st mode we get a mass sensitivity $S_{1st} = (5.5 \pm 0.3) Hz\ ng^{-1}$. The diaphragm has then the potential to be used as mass microbalance. In future works we keep using certified microbeads to study the sensitivity stability of the device and we will extend our study directly to particulate matter weighing.

2.3.2 PM module

As part of the detection of atmospheric particulate matter for PM2.5 and PM10, which is one of the main objectives of the project S.A.L.VO., we introduce a mock-up for a sensor capable of measuring the concentration of

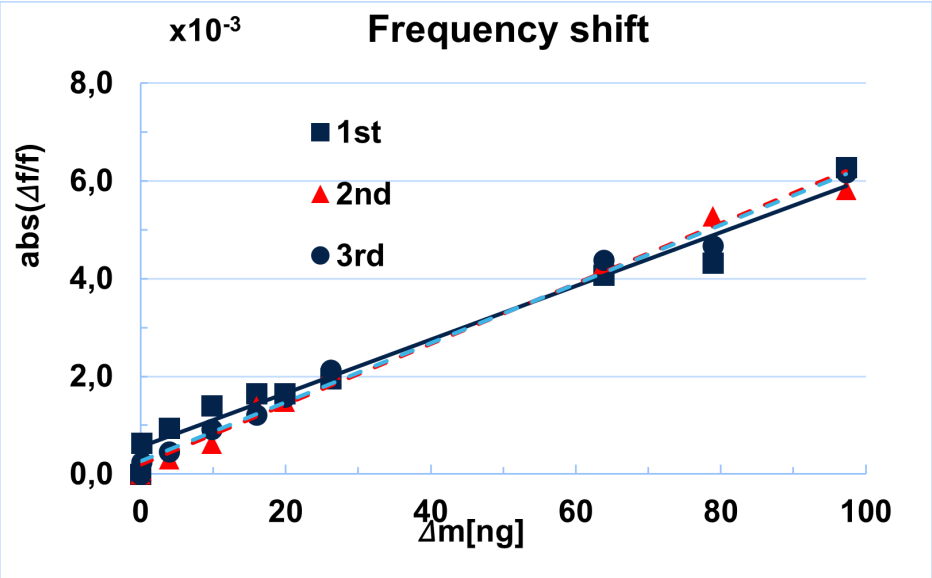

Figure 2.18: Measured resonance frequency shift (%) at each mass loading step. The figure show: 1st mode shift in black-square; 2nd mode shift in red triangle; 3rd mode shift blue circle

these pollutants.

The sensor is based on a gravimetric method [66]. The sensing body is made of a circular membrane of piezoelectric material, of PZT [67, 68] (lead-titanium zirconate), which vibrates at a resonance frequency around 250 kHz. The particulate matter deposited on the membrane decreases its resonance frequency [69, 70]. The recorded frequency shift can therefore be correlated to the deposited mass [71]. Knowing the flow that crosses the chamber, where this sensitive body is inserted, we have in fact information on the concertation of particulate present in the air.

As can be seen from Figure 2.19, the mock-up is a self-consistent set of several devices. There is a module for reading the signal that then gives us information on the resonance frequency recorded, there is a module for controlling the flow, generated by a piezoelectric pump, and the temperature of the heater present in the PM cell, parameters that must be set in such a way as to maximize the efficiency of deposition [72] of PM on the sensitive body, and the PM cell itself where the sensitive membranes are housed. The

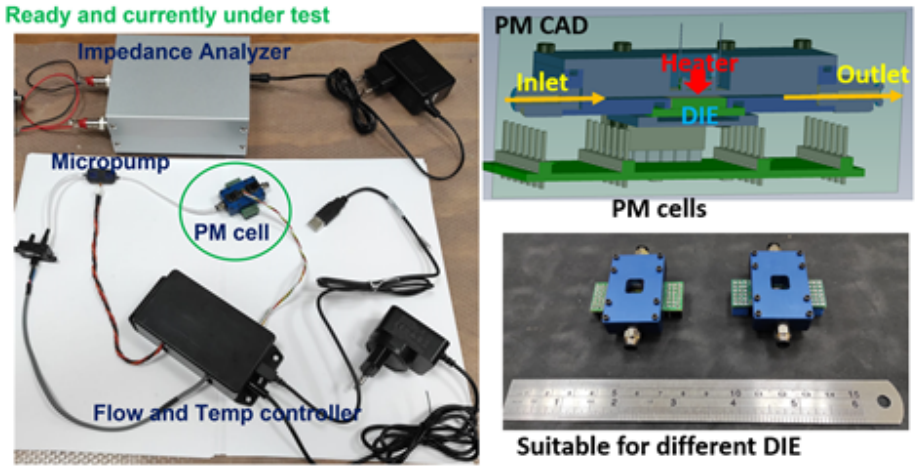

Figure 2.19: PM mock up. (a) components that make up the sensor (b) CAD of the PM cell and the driver board, (c) a picture of the PM cells.

principle of measurement is to sample air with a constant flow, and after ts (sampling time) to record the frequency variation. The sampled air volume is obtained by measuring the air flow thorough the device while the deposited particulate matter mass is indirectly evaluated by the frequency shift. Each information allows us to get the concentration of particulate matter in the sampled air volume. Being the chamber of small size, the sampled volume is low and small amounts of PM can reach the sensing membrane. However, the high sensitivity of the piezoelectric sensing membrane (10 Hz/ng) allow to measure small amount of PM in line with such small sampled volume. Higher sampled volume can be obtained by increasing the air flow. Anyway, the PM deposition rate onto the membrane is dependent on the heater temperature at each given air flow setpoint and higher flow rate provided unstable acquisition. A full data set was explored by changing the flow setpoint and heater temperature. Particulate chamber tests (ENEA) confirm the deposition of the material on the sensing surface, as can be seen in figure 2.20.

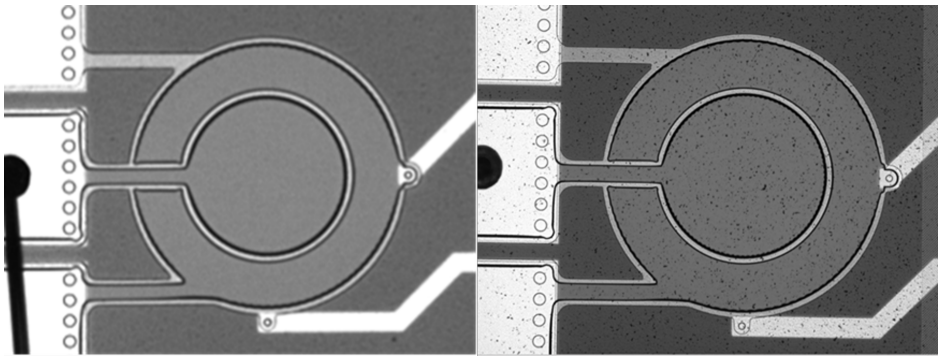

Figure 2.20: Pictures before and after PM deposition on the sensing membrane downstream of a particulate chamber test.

CONCLUSION

This thesis was developed within S.A.L.VO. A substantial part of the thesis, carried out at the laboratories of the ENEA research center in Portici (NA), concerned the study of the regulations relating to the concentration limits of atmospheric particulate and the related monitoring technologies, then resulted in the construction of a test chamber for particulate matter in the ENEA research center in Portici, which was one of the major objectives achieved within the project. The validation phase of the test chamber was carried out on commercial particulate sensors, also in order to evaluate their use in the prototype envisaged by the project; the parameters measured in the test chamber were found to be in line with those present in the literature, thus confirming the functioning of the test chamber. A second phase of the experimental work involved the feasibility study in the use of piezoelectric materials as MEMS sensors for the development of new particulate sensors. This part of the work is still being completed, as the project is still in progress: at the moment the functioning of the MEMS sensors as microbalances has been successfully tested, to then move on to the design and implementation of a first self-consistent mock-up for the measurement of the particulate matter. The results obtained in the ENEA particulate test chamber confirmed the deposition of PM on the sensor surface and frequency shifts are visible. In the continuation of the project, a second realization of a new mock-up is planned to improve the criticalities of the previous one.

BIBLIOGRAPHY

[1] B. Alfano, L. Barretta, A. Del Giudice, S. De Vito, G. Di Francia, E. Esposito, F. Formisano, E. Massera, M. L. Miglietta, and T. Polichetti, "A review of low-cost particulate matter sensors from the developers' perspectives," *Sensors*, vol. 20, no. 23, p. 6819, 2020.

[2] K. Kuklinska, L. Wolska, and J. Namiesnik, "Air quality policy in the us and the eu–a review," *Atmospheric Pollution Research*, vol. 6, no. 1, pp. 129–137, 2015.

[3] R. Esworthy, "Air quality: Epa's 2013 changes to the particulate matter (pm) standard," 2013.

[4] E. protection agency, "Revisions to the national ambient air quality standards for particulate matter." `https://www.epa.gov/sites/default/files/2020-07/documents/pm-1987-final-52fr246341.pdf`, 1987. [Online; accessed 01-April-2022].

[5] R. O. McClellan, "Setting ambient air quality standards for particulate matter," *Toxicology*, vol. 181, pp. 329–347, 2002.

[6] G. Snider, C. L. Weagle, K. K. Murdymootoo, A. Ring, Y. Ritchie, E. Stone, A. Walsh, C. Akoshile, N. X. Anh, R. Balasubramanian, J. Brook, F. D. Qonitan, J. Dong, D. Griffith, K. He, B. N. Holben, R. Kahn, N. Lagrosas, P. Lestari, Z. Ma, A. Misra, L. K. Norford, E. J. Quel, A. Salam, B. Schichtel, L. Segev, S. Tripathi, C. Wang, C. Yu,

Q. Zhang, Y. Zhang, M. Brauer, A. Cohen, M. D. Gibson, Y. Liu, J. V. Martins, Y. Rudich, and R. V. Martin, "Variation in global chemical composition of $pm_{2.5}$: emerging results from spartan," *Atmospheric Chemistry and Physics*, vol. 16, no. 15, pp. 9629–9653, 2016.

[7] EEA, "Air quality in europe." `https://www.eea.europa.eu/publications/air-quality-in-europe2018`, 2018. [Online; accessed 01-April-2022].

[8] J. L. Mauderly and J. C. Chow, "Health effects of organic aerosols," *Inhalation toxicology*, vol. 20, no. 3, pp. 257–288, 2008.

[9] J. L. Mauderly, "Diesel emissions: is more health research still needed?," *Toxicological Sciences*, vol. 62, no. 1, pp. 6–9, 2001.

[10] C. L. Wiseman and F. Zereini, "Airborne particulate matter, platinum group elements and human health: a review of recent evidence," *Science of the Total Environment*, vol. 407, no. 8, pp. 2493–2500, 2009.

[11] JRC, "Source profiles for europe database." `https://source-apportionment.jrc.ec.europa.eu/Specieurope/sources.aspx`. [Online; accessed 01-April-2022].

[12] EC, "Guidance on $pm_{2.5}$ measurement under directive 1999/30/ec.." `https://ec.europa.eu/environment/archives/cafe/pdf/steering_technical_group/guidancepm.pdf`, 1999. [Online; accessed 01-April-2022].

[13] J. Gilliam and E. Hall, "Reference and equivalent methods used to measure national ambient air quality standards (naaqs) criteria air pollutants-volume ius environmental protection agency, washington, dc," *Environmental Protection Agency: Washington, DC, USA*, 2016.

[14] E. S. Hall, S. M. Kaushik, R. W. Vanderpool, R. M. Duvall, M. R. Beaver, R. W. Long, and P. A. Solomon, "Integrating sensor monitoring technology into the current air pollution regulatory support paradigm:

Practical considerations," *Am. J. Environ. Eng*, vol. 4, no. 6, pp. 147–154, 2014.

[15] C. M. Sorensen, J. Gebhart, T. J. O'Hern, and D. J. Rader, *Optical measurement techniques: fundamentals and applications*. John Wiley & Sons, Inc, 2011.

[16] G. Mie, "Beiträge zur optik trüber medien, speziell kolloidaler metallösungen," *Annalen der physik*, vol. 330, no. 3, pp. 377–445, 1908.

[17] K. Wang, F.-e. Chen, W. Au, Z. Zhao, and Z.-l. Xia, "Evaluating the feasibility of a personal particle exposure monitor in outdoor and indoor microenvironments in shanghai, china," *International journal of environmental health research*, vol. 29, no. 2, pp. 209–220, 2019.

[18] V. Papapostolou, H. Zhang, B. J. Feenstra, and A. Polidori, "Development of an environmental chamber for evaluating the performance of low-cost air quality sensors under controlled conditions," *Atmospheric Environment*, vol. 171, pp. 82–90, 2017.

[19] A. Cavaliere, F. Carotenuto, F. Di Gennaro, B. Gioli, G. Gualtieri, F. Martelli, A. Matese, P. Toscano, C. Vagnoli, and A. Zaldei, "Development of low-cost air quality stations for next generation monitoring networks: Calibration and validation of pm2. 5 and pm10 sensors," *Sensors*, vol. 18, no. 9, p. 2843, 2018.

[20] N. Chigier and G. Stewart, "Guest editorial particle sizing and spray analysis," *Optical engineering*, vol. 23, no. 5, p. 235554, 1984.

[21] I. Agranovski, *Aerosols: Science and technology*. John Wiley & Sons, 2011.

[22] M. Carratù, M. Ferro, V. Paciello, P. Sommella, J. Lundgren, and M. O'Nils, "Wireless sensor network calibration for pm10 measurement," in *2020 IEEE International Conference on Computational Intelligence and Virtual Environments for Measurement Systems and Applications (CIVEMSA)*, pp. 1–6, IEEE, 2020.

[23] Y. Wang, J. Li, H. Jing, Q. Zhang, J. Jiang, and P. Biswas, "Laboratory evaluation and calibration of three low-cost particle sensors for particulate matter measurement," *Aerosol science and technology*, vol. 49, no. 11, pp. 1063–1077, 2015.

[24] E. Austin, I. Novosselov, E. Seto, and M. G. Yost, "Laboratory evaluation of the shinyei ppd42ns low-cost particulate matter sensor," *PloS one*, vol. 10, no. 9, p. e0137789, 2015.

[25] S. Sousan, K. Koehler, G. Thomas, J. H. Park, M. Hillman, A. Halterman, and T. M. Peters, "Inter-comparison of low-cost sensors for measuring the mass concentration of occupational aerosols," *Aerosol Science and Technology*, vol. 50, no. 5, pp. 462–473, 2016.

[26] D. A. Hapidin, C. Saputra, D. S. Maulana, M. M. Munir, K. Khairurrijal, *et al.*, "Aerosol chamber characterization for commercial particulate matter (pm) sensor evaluation," *Aerosol and Air Quality Research*, vol. 19, no. 1, pp. 181–194, 2019.

[27] K.-H. Ahn, H. Lee, H. D. Lee, and S. C. Kim, "Extensive evaluation and classification of low-cost dust sensors in laboratory using a newly developed test method," *Indoor air*, vol. 30, no. 1, pp. 137–146, 2020.

[28] H. Omidvarborna, P. Kumar, and A. Tiwari, "'envilution™'chamber for performance evaluation of low-cost sensors," *Atmospheric Environment*, vol. 223, p. 117264, 2020.

[29] F. M. J. Bulot, H. S. Russell, M. Rezaei, M. S. Johnson, S. J. J. Ossont, A. K. R. Morris, P. J. Basford, N. H. C. Easton, G. L. Foster, M. Loxham, *et al.*, "Laboratory comparison of low-cost particulate matter sensors to measure transient events of pollution," *Sensors*, vol. 20, no. 8, p. 2219, 2020.

[30] R. J. Vercellino, D. K. Sleeth, R. G. Handy, K. T. Min, and S. C. Collingwood, "Laboratory evaluation of a low-cost, real-time, aerosol multisensor," *Journal of occupational and environmental hygiene*, vol. 15, no. 7, pp. 559–567, 2018.

[31] A. John and P. Joseph, "Wireless air quality and emission monitoring," 2016.

[32] V. B. Mikheev, A. Ivanov, E. A. Lucas, P. L. South, H. O. Colijn, and P. I. Clark, "Aerosol size distribution measurement of electronic cigarette emissions using combined differential mobility and inertial impaction methods: Smoking machine and puff topography influence," *Aerosol Science and Technology*, vol. 52, no. 11, pp. 1233–1248, 2018.

[33] J.-F. Bertholon, M.-H. Becquemin, M. Roy, F. Roy, D. Ledur, I. Annesi-Maesano, and B. Dautzenberg, "Particle sizes of aerosols produced by nine indoor perfumes and deodorants," *Int. J. Environ. Monit. Anal*, vol. 3, pp. 377–381, 2015.

[34] K. K. Johnson, M. H. Bergin, A. G. Russell, and G. S. Hagler, "Using low cost sensors to measure ambient particulate matter concentrations and on-road emissions factors," *Atmospheric Measurement Techniques Discussions*, pp. 1–22, 2016.

[35] M. Levy Zamora, F. Xiong, D. Gentner, B. Kerkez, J. Kohrman-Glaser, and K. Koehler, "Field and laboratory evaluations of the low-cost plantower particulate matter sensor," *Environmental science & technology*, vol. 53, no. 2, pp. 838–849, 2018.

[36] G. Mainelis, D. Berry, H. R. An, M. Yao, K. DeVoe, D. E. Fennell, and R. Jaeger, "Design and performance of a single-pass bubbling bioaerosol generator," *Atmospheric environment*, vol. 39, no. 19, pp. 3521–3533, 2005.

[37] C. Terzano, "Metered dose inhalers and spacer devices," *European review for medical and pharmacological sciences*, vol. 3, pp. 159–170, 1999.

[38] R. Zhang, X. Song, S. Zhan, J. Hu, and W. Tan, "Investigation of influence factors on particle size measurement with pmdi.," *Biomedical Research (0970-938X)*, vol. 28, no. 21, 2017.

[39] T. Sayahi, A. Butterfield, and K. Kelly, "Long-term field evaluation of the plantower pms low-cost particulate matter sensors," *Environmental pollution*, vol. 245, pp. 932–940, 2019.

[40] F. M. Bulot, S. J. Johnston, P. J. Basford, N. H. Easton, M. Apetroaie-Cristea, G. L. Foster, A. K. Morris, S. J. Cox, and M. Loxham, "Long-term field comparison of multiple low-cost particulate matter sensors in an outdoor urban environment," *Scientific reports*, vol. 9, no. 1, pp. 1–13, 2019.

[41] M. Badura, P. Batog, A. Drzeniecka-Osiadacz, and P. Modzel, "Evaluation of low-cost sensors for ambient pm2. 5 monitoring," *Journal of Sensors*, vol. 2018, 2018.

[42] M. Alvarado, F. Gonzalez, A. Fletcher, and A. Doshi, "Towards the development of a low cost airborne sensing system to monitor dust particles after blasting at open-pit mine sites," *Sensors*, vol. 15, no. 8, pp. 19667–19687, 2015.

[43] AQSPEC, "Field test protocols." `http://www.aqmd.gov/docs/default-source/aq-spec/protocols/sensors-field-testing-protocol.pdf?sfvrsn=0`. [Online; accessed 01-April-2022].

[44] AQSPEC, "Pm sensing performance report.." `http://www.aqmd.gov/aq-spec/evaluations/summary-pm`. [Online; accessed 01-April-2022].

[45] P. K. Rai, "Multifaceted health impacts of particulate matter (pm) and its management: an overview," *Environmental Skeptics and Critics*, vol. 4, no. 1, p. 1, 2015.

[46] EPA, "Air sensor toolbox.." `https://www.epa.gov/air-sensor-toolbox`. [Online; accessed 01-April-2022].

[47] S. Feinberg, R. Williams, G. S. Hagler, J. Rickard, R. Brown, D. Garver, G. Harshfield, P. Stauffer, E. Mattson, R. Judge, *et al.*, "Long-term evaluation of air sensor technology under ambient conditions in denver, col-

orado," *Atmospheric measurement techniques*, vol. 11, no. 8, pp. 4605–4615, 2018.

[48] I. Han, E. Symanski, and T. H. Stock, "Feasibility of using low-cost portable particle monitors for measurement of fine and coarse particulate matter in urban ambient air," *Journal of the Air & Waste Management Association*, vol. 67, no. 3, pp. 330–340, 2017.

[49] L. R. Crilley, M. Shaw, R. Pound, L. J. Kramer, R. Price, S. Young, A. C. Lewis, and F. D. Pope, "Evaluation of a low-cost optical particle counter (alphasense opc-n2) for ambient air monitoring," *Atmospheric Measurement Techniques*, vol. 11, no. 2, pp. 709–720, 2018.

[50] A. Mukherjee, L. G. Stanton, A. R. Graham, and P. T. Roberts, "Assessing the utility of low-cost particulate matter sensors over a 12-week period in the cuyama valley of california," *Sensors*, vol. 17, no. 8, p. 1805, 2017.

[51] S. J. Johnston, P. J. Basford, F. M. Bulot, M. Apetroaie-Cristea, N. H. Easton, C. Davenport, G. L. Foster, M. Loxham, A. K. Morris, and S. J. Cox, "City scale particulate matter monitoring using lorawan based air quality iot devices," *Sensors*, vol. 19, no. 1, p. 209, 2019.

[52] S. N. Feinberg, R. Williams, G. Hagler, J. Low, L. Smith, R. Brown, D. Garver, M. Davis, M. Morton, J. Schaefer, *et al.*, "Examining spatiotemporal variability of urban particulate matter and application of high-time resolution data from a network of low-cost air pollution sensors," *Atmospheric environment*, vol. 213, pp. 579–584, 2019.

[53] A. Di Antonio, O. A. Popoola, B. Ouyang, J. Saffell, and R. L. Jones, "Developing a relative humidity correction for low-cost sensors measuring ambient particulate matter," *Sensors*, vol. 18, no. 9, p. 2790, 2018.

[54] S. Sousan, K. Koehler, L. Hallett, and T. M. Peters, "Evaluation of the alphasense optical particle counter (opc-n2) and the grimm portable aerosol spectrometer (pas-1.108)," *Aerosol Science and Technology*, vol. 50, no. 12, pp. 1352–1365, 2016.

[55] C. Báthory, M. L. Kiss, A. Trohák, Z. Dobó, and Á. B. Palotás, "Preliminary research for low-cost particulate matter sensor network," in *E3S Web of Conferences*, vol. 100, p. 00004, EDP Sciences, 2019.

[56] "Topas sag 410." `https://www.topas-gmbh.de/en/produkte/sag-410/`. [Online; accessed 01-April-2022].

[57] "Dusttrak™ drx aerosol monitor 8533." `https://tsi.com/products/aerosol-and-dust-monitors/dust-monitors/dusttrak%e2%84%a2-drx-aerosol-monitor-8533/`. [Online; accessed 01-April-2022].

[58] L. Barretta, E. Massera, B. Alfano, T. Polichetti, M. Miglietta, P. Maddalena, F. Foncellino, F. Formisano, S. D. Vito, E. Esposito, *et al.*, "Study and characterization of lcpms in the laboratory," in *AISEM Annual Conference on Sensors and Microsystems*, pp. 175–181, Springer, 2020.

[59] R. Williams, D. Nash, G. Hagler, K. Benedict, I. MacGregor, B. Seay, M. Lawrence, T. Dye, *et al.*, "Peer review and supporting literature review of air sensor technology performance targets," *Washington, DC: Environmental Protection Agency*, 2018.

[60] A. Meitzler, H. Tiersten, A. Warner, D. Berlincourt, G. Couqin, and F. Welsh III, "Ieee standard on piezoelectricity "ansi/ieee std 176–1987"," *The Institute of Electrical and Electronics Engineers Inc*, 1987.

[61] H. Choi, *Fabrication, characterization and modeling of K (31) piezoelectric Micromachined Ultrasonic Transducers(pMUTs)*, vol. 69. 2007.

[62] S. Tadigadapa, "Piezoelectric microelectromechanical systems—challenges and opportunities," *Procedia Engineering*, vol. 5, pp. 468–471, 2010.

[63] D. Damjanovic, "Ferroelectric, dielectric and piezoelectric properties of ferroelectric thin films and ceramics," *Reports on Progress in Physics*, vol. 61, no. 9, p. 1267, 1998.

[64] Y. Lu, *Piezoelectric micromachined ultrasonic transducers for fingerprint sensing*. University of California, Davis, 2015.

[65] A. Dangi and R. Pratap, "System level modeling and design maps of pmuts with residual stresses," *Sensors and Actuators A: Physical*, vol. 262, pp. 18–28, 2017.

[66] V. Tasić, M. Jovašević-Stojanović, S. Vardoulakis, N. Milošević, R. Kovačević, and J. Petrović, "Comparative assessment of a real-time particle monitor against the reference gravimetric method for pm_{10} and $pm_{2.5}$ in indoor air," 2012.

[67] A. Ismail, J. Burdess, A. Harris, C. McNeil, J. Hedley, S. Chang, and G. Suarez, "The principle of a mems circular diaphragm mass sensor," *Journal of micromechanics and microengineering*, vol. 16, no. 8, p. 1487, 2006.

[68] F. Foncellino, L. Barretta, and E. Massera, "Concept of mems vibrating membrane as particulate matter (pm) sensor," in *AISEM Annual Conference on Sensors and Microsystems*, pp. 119–123, Springer, 2020.

[69] H. Nazemi, J. Antony Balasingam, S. Swaminathan, K. Ambrose, M. U. Nathani, T. Ahmadi, Y. Babu Lopez, and A. Emadi, "Mass sensors based on capacitive and piezoelectric micromachined ultrasonic transducers—cmut and pmut," *Sensors*, vol. 20, no. 7, 2020.

[70] Z. Wang, J. Miao, T. Xu, L. Yu, C. M. Li, and X. Chen, "Biosensors based on flexural mode piezo-diaphragm," in *2008 3rd IEEE International Conference on Nano/Micro Engineered and Molecular Systems*, pp. 374–378, 2008.

[71] F. Foncellino, L. Barretta, E. Massera, and A. Corigliano, "Piezoelectric mems for microparticles detection," in *2021 IEEE Sensors*, pp. 1–4, 2021.

[72] D. Fahimi, O. Mahdavipour, J. Sabino, R. M. White, and I. Paprotny, "Vertically-stacked mems pm2.5 sensor for wearable applications," *Sensors and Actuators A: Physical*, vol. 299, p. 111569, 2019.